

pubs.acs.org/JPCC Article

# Parallel Alkane Dehydrogenation Routes on Brønsted Acid and Reaction-Derived Carbonaceous Active Sites in Zeolites

Philip M. Kester, Enrique Iglesia, and Rajamani Gounder\*



Cite This: J. Phys. Chem. C 2020, 124, 15839-15855



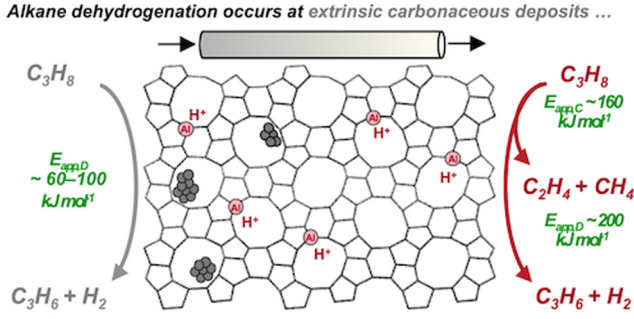
**ACCESS** 

III Metrics & More

Article Recommendations

Supporting Information

ABSTRACT: Alkane dehydrogenation rates on acidic zeolites measured in the presence of co-fed H<sub>2</sub> during initial contact with reactants solely reflect protolytic reactions at Brønsted acid sites, while rates measured without co-fed H<sub>2</sub> and at later reaction times reflect additional contributions from an extrinsic dehydrogenation function derived from reactants and products. This extrinsic function consists of unsaturated organic residues that catalyze dehydrogenation turnovers by accepting H-atoms from alkanes and recombining them as H<sub>2</sub>. Such hydrogen transfer routes are inhibited by alkenes and H<sub>2</sub> products and proceed with activation barriers much lower than for protolytic dehydrogenation at H<sup>+</sup> sites, causing them to become more prevalent at lower temperatures and for zeolites with lower H<sup>+</sup> densities. The number,



... and prevails at lower temperatures, H\* contents, and product pressures

composition, and reactivity of these extrinsic carbonaceous active sites depend on the local concentrations of reactants and products, which vary with alkane and H<sub>2</sub> pressure, bed residence time, and axial mixing. These extrinsic catalytic moieties form within H<sub>2</sub>-deficient regions of catalyst beds but can be removed by thermal treatments in H<sub>2</sub>, which fully restore zeolite catalysts to their initial state. Carbonaceous deposits do not catalyze alkane cracking reactions; thus, cracking rate constants serve as a reporter of the state of proton sites, and their invariance with product pressure, residence time, and axial mixing confirms that protons remain unoccupied and undisturbed as extrinsic organic residues change in number, composition, and reactivity. The rates of the reverse reaction (alkene hydrogenation) under H<sub>2</sub>-rich conditions inhibit the formation and the reactivity of these organic residues, and taken together with formalisms based on nonequilibrium thermodynamics, they confirm that alkane dehydrogenation occurs solely via protolytic routes only at the earliest stages of reaction in the presence of added H<sub>2</sub>. These findings provide a coherent retrospective view of the root causes of the literature discord about alkane dehydrogenation turnover rates and activation barriers on acidic zeolites, variously attributed to extraframework Al or radical active sites and to turnovers limited by alkene desorption instead of protolytic steps. Importantly, these findings also prescribe experimental protocols that isolate the kinetic contributions of protolytic dehydrogenation routes, thus ensuring their replication, while suggesting strategies to deposit or remove extrinsic organocatalytic functions that mediate hydrogen transfer reactions.

## 1. INTRODUCTION

Zeolites and microporous solid acids are ubiquitous in the catalytic conversion of light alkanes to alkenes via dehydrogenation and cracking reactions and in the subsequent conversion of alkenes to larger hydrocarbons via oligomerization,<sup>2,3</sup> alkylation,<sup>4</sup> and aromatization<sup>5</sup> reactions. Brønsted acid sites are present in aluminosilicate zeolites in their proton forms as hydroxyl groups that bridge framework Si and Al atoms, where the proton balances the negative charge created by substituting Al for Si. These protons react with C-C or C-H bonds in alkanes to form penta-coordinated  $(C-C-H)^+$  or  $(C-H-H)^+$ carbonium-ion-like transition states in monomolecular (i.e., protolytic) cracking and dehydrogenation pathways, respectively.6 Protolytic alkane reactions tend to prevail at high temperatures (>623 K) and low conversions (<2%) because alkenes initiate more facile bimolecular cracking routes that are mediated by carbenium-ion transition states<sup>7,8</sup> and thus prevail at higher conversions (i.e., product alkene pressures) and lower temperatures. The kinetic signatures of protolytic alkane activation are evident in measured barriers for first-order cracking and dehydrogenation rate constants that differ by the ensemble-averaged proton affinity among the different C–C and C–H bonds in gaseous alkane reactants, according to Born–Haber thermochemical cycle analyses; <sup>9–11</sup> in the case of propane, measured activation barriers are 25–40 kJ mol<sup>-1</sup> higher for dehydrogenation (185–200 kJ mol<sup>-1</sup>) than for

Received: February 29, 2020 Revised: April 30, 2020 Published: June 16, 2020





cracking (160 kJ mol<sup>-1</sup>). Protolytic alkane dehydrogenation routes also prevail on zeolites that do not contain other active site functions, such as metals<sup>12-17</sup> and cations<sup>18,19</sup> that are purposely introduced or present as adventitious impurities. When such functions are also present, the carbonium-ion-like transition states that form at proton sites cause them to behave as a less competent function for activating C–H bonds in alkane dehydrogenation reactions.

Previous studies of propane reactions on H-form zeolites at conditions that tend to favor protolytic pathways (675-875 K, 2-10 kPa  $C_3H_8$ )<sup>9,22-26</sup> have reported activation barriers that vary widely for dehydrogenation (65-202 kJ mol<sup>-1</sup>; Table S1, SI) but that are quite similar in all studies for cracking (147-165 kJ mol<sup>-1</sup>; Table S1, SI), suggesting that dehydrogenation at non-protonic sites may also occur at certain conditions or on a subset of these nominally similar catalysts. Narbeshuber et al. measured an H/D kinetic isotope effect (KIE) of 1.7 (at 773 K) for *n*-butane cracking (the ratio of rates for n-C<sub>4</sub>H<sub>10</sub> and n- $C_4D_{10}$  reactants) on H-MFI (Si/Al = 35) that would be consistent with kinetically relevant proton insertion into alkane C–C bonds, but a measured KIE value of only 1.1 for *n*-butane dehydrogenation.<sup>22</sup> Such low KIE values for nC<sub>4</sub> dehydrogenation, together with the measured activation barriers for C<sub>3</sub>-C<sub>6</sub> n-alkane dehydrogenation that increased systematically with carbon chain length (95-160 kJ mol<sup>-1</sup>), suggested that steps other than proton insertion into alkane C-H bonds were relevant for dehydrogenation events.<sup>22</sup> These observations were interpreted in terms of alkene desorption from bound alkoxides as the sole kinetically relevant dehydrogenation step,<sup>27</sup> as also invoked by van Bokhoven and co-workers to rationalize propane dehydrogenation barriers of 123-178 kJ mol<sup>-1</sup> measured on H-form zeolites with different framework topologies (\*BEA, MOR, MFI, FAU; 675-875 K). 23,24 The kinetic relevance of alkene desorption, however, requires relevant coverages of alkoxides and thus rate inhibition by alkene products, which were not reported in these studies. At first glance, such a proposal would appear consistent with the observations by Janda and Bell that *n*-butane dehydrogenation rates (773 K) on H-MFI (Si/Al = 12) were lower when butenes were added to the reactant stream;<sup>28</sup> yet, product inhibition of acid sites should have also inhibited cracking rates and caused dehydrogenation rates to become less than firstorder in alkane pressure, in contradiction with their reported first-order dependence of rates on alkane pressure. These proposals were shown to be incorrect by Li and co-workers; their infrared spectra collected in operando during n-butane reactions on H-MFI (Si/Al = 29) at 618-710 K did not detect any changes in the intensity or frequency of the acidic OH stretches (~3600 cm<sup>-1</sup>) with changes in bed residence time, which led to concomitant changes in dehydrogenation rates, presumably as a result of changes in the prevalent product concentrations.<sup>26</sup> These observations indicate that products must inhibit dehydrogenation reactions at another active function that is distinct from protons and that non-protonic functions lead to measured activation energies (90 kJ mol<sup>-1</sup>) and entropies (-190 J mol<sup>-1</sup> K<sup>-1</sup>) for propane dehydrogenation<sup>26</sup> that differ significantly from those expected for protolytic pathways from Born-Haber thermochemical cycle analyses (200 kJ mol<sup>-1</sup> and -60 J mol<sup>-1</sup> K<sup>-1</sup>, respectively).

The identity of non-protonic alkane dehydrogenation active sites on zeolites has been the subject of broad speculation, leading to proposals that extraframework Al species can act as Lewis acid centers that mediate such reactions<sup>29</sup> and that

homolytic O–H cleavage at high temperatures (~1073 K) in inert environments forms radical species at lattice O atoms that mediate such reactions,<sup>30</sup> all without compelling theoretical or experimental evidence. These alternate active site proposals were invoked in studies that reported activation barriers for propane dehydrogenation that varied widely (84–187 kJ mol<sup>-1</sup>) and were much lower than expected for protolytic pathways (200 kJ mol<sup>-1</sup>). These studies collectively suggest that non-protonic active sites contribute to dehydrogenation events, but the identity and genesis of such active sites remain unclear. Non-protolytic alkane dehydrogenation pathways are typically attributed to active functions derived from structures inherent to aluminosilicate zeolites and not from structures derived from reactants as extrinsic components that reside within (but are not an intrinsic part of) zeolite voids.

This study reports evidence that propane dehydrogenation rates (718-778 K) during initial contact with reactants on Hform zeolites pretreated in H2 and measured in differential reactors (i.e., with alkene and H<sub>2</sub> products co-fed) solely reflect protolytic alkane activation at Brønsted acid sites. In sharp contrast, steady-state propane dehydrogenation rates measured in the absence of co-fed products are inhibited by propene and H<sub>2</sub> and occur via pathways with measured barriers that are significantly lower (by 100-150 kJ mol<sup>-1</sup>) than those for protolytic dehydrogenation (~200 kJ mol<sup>-1</sup>); propane cracking rates measured simultaneously and arising only from protolytic pathways at H<sup>+</sup> sites are not inhibited by products. Propane reactants and/or their propene products form unsaturated organic residues within zeolite voids when H<sub>2</sub> pressures are low, and such residues can transfer hydrogen atoms with propane to form propene and then can desorb H<sub>2</sub> to restore their unsaturation, thus behaving as catalytic sites for alkane dehydrogenation. The kinetic behavior of reactionderived carbonaceous deposits extrinsic to zeolite surfaces provides a unifying explanation for the origin of non-protolytic alkane dehydrogenation observed on acidic zeolites among discordant literature reports over the past few decades. This work also establishes experimental protocols to avoid corruptions caused by carbonaceous deposits in studies of the intrinsic catalytic properties of acidic zeolites.

# 2. EXPERIMENTAL METHODS

2.1. Synthesis and Treatments of Zeolites. MFI (CBV3024E, CBV8014, CBV28014) and MOR (CBV21A) zeolites were obtained from Zeolyst International in NH<sub>4</sub>-form and converted to their H-form via treatment in flowing dry air (1.67 cm<sup>3</sup> s<sup>-1</sup> (g solid)<sup>-1</sup>, UHP, 99.999%, Indiana Oxygen) to 773 K  $(0.0167 \text{ K s}^{-1})$  for 4 h. CHA zeolites were synthesized according to the procedures reported by Di Iorio and Gounder<sup>31</sup> from a solution with a molar composition of 1 SiO<sub>2</sub>/0.067 Al(OH)<sub>3</sub>/0.5 TMAdaOH/44 H<sub>2</sub>O, where TMAdaOH refers to N,N,N-trimethyl-1-adamantylammonium hydroxide (1 M TMAdaOH solution; 25 wt%, Sachem). This solution was subjected to a crystallization procedure at 433 K (under rotation at 30 rpm) for 144 h. The solids formed were washed with deionized water and acetone (>99.5 wt %, Sigma-Aldrich) in alternate washes (30 cm<sup>3</sup> (g solid)<sup>-1</sup> per wash) until the pH of the supernatant solution was constant  $(\sim 7.5)$ . The washed solids were then separated by centrifugation, treated in ambient air at 373 K for 24 h and then in flowing dry air  $(1.67 \text{ cm}^3 \text{ s}^{-1} \text{ (g solid)}^{-1}, \text{ UHP}, 99.999\%$ , Indiana Oxygen) to 853 K  $(0.0167 \text{ K s}^{-1})$ , and held for 10 h to remove the organic species occluded during hydrothermal synthesis protocols. CHA samples were subsequently converted to their NH<sub>4</sub>-form by aqueous-phase ion exchange (100 cm³ (g solid) $^{-1}$ ) in a 1 M NH<sub>4</sub>NO<sub>3</sub> solution (8.0 wt% in deionized H<sub>2</sub>O; 99.9 wt%, Sigma-Aldrich) for 24 h under ambient conditions and then washed 4 times in deionized water (30 cm³ (g solid) $^{-1}$  per wash) and recovered via centrifugation. NH<sub>4</sub>-CHA was converted to H-CHA via the same method as used for converting NH<sub>4</sub>-form MFI and MOR zeolites to their H-form. Samples are denoted XXX–Y, where XXX is the three-letter framework code and Y is the solid Si/Al ratio.

**2.2.** Structural and Textural Properties of Zeolite Samples. Crystal structures were confirmed by powder X-ray diffractograms (XRD) collected using a Rigaku Smartlab X-ray diffractometer equipped with a Cu K $\alpha$  radiation source operating at 1.76 kW. In typical experiments, the samples (0.01 g) were loaded into a zero-background low-dead-volume sample holder (Rigaku) and diffractograms were collected over a 4–40°  $2\theta$  range with a step size of 0.01° and a scan rate of 0.0167° s<sup>-1</sup>.

Micropore volumes of MFI and MOR zeolites were determined from N<sub>2</sub> uptakes (77 K; Micromeritics ASAP 2020 surface area and porosity analyzer). H-MFI and H-MOR samples (0.03–0.05 g, pelleted and sieved to 180–250  $\mu$ m) were evacuated by heating to 393 K (0.167 K s<sup>-1</sup>) in a dynamic vacuum (6.7 mbar) for 2 h and then heating to 623 K (0.167 K  $s^{-1}$ ) and holding for 9 h. Volumetric uptakes of  $N_2$  at relative pressures of  $0.05-0.35 P/P_0$  were linearly extrapolated to zero relative pressure to estimate the micropore volumes (cm<sup>3</sup> (STP) g<sup>-1</sup>). Micropore volumes of H-CHA zeolites were determined from Ar adsorption isotherms (87 K) measured using procedures similar to those used for N2 adsorption isotherms and were similar to those estimated from the semilogarithmic derivative plot of the adsorption isotherm given by  $\partial(V_{ads})/\partial(\ln(P/P_0))$  vs  $\ln(P/P_0)$ . All reported micropore volumes were similar (within 10%) between these two methods.

The Al content in MFI, MOR, and CHA zeolites was measured by atomic absorption spectroscopy (AAS) using a PerkinElmer model AAnalyst 300 atomic absorption spectrometer, and the Si/Al ratio for each sample was calculated from the unit cell formula. The samples were prepared for analysis by adding a 2g HF (48 wt%, Alfa Aesar) to ~0.02 g of sample and allowing the sample to dissolve for 3 days at ambient temperature. The HF acid solution was then diluted with 50 g of deionized water. [Caution: when working with HF acid, use appropriate personal protective equipment, ventilation, and other safety precautions] Absorbances were measured using a wavelength of 309.3 nm in a reducing acetylene/nitrous oxide flame. Elemental compositions were calculated from calibration curves generated from standard solutions.

The number of acidic protons was determined from the amount of NH<sub>3</sub> evolved during the thermal treatment of samples in their NH<sub>4</sub>-form (NH<sub>3</sub> TPD) using a Micromeritics AutoChem II 2920 Chemisorption analyzer and an Agilent 5973N mass-selective detection system to identify gaseous products evolved from zeolite samples. NH<sub>4</sub>-form zeolites (0.02–0.05 g) were loaded into a U-shaped quartz reactor, supported with quartz wool, and placed in a clam-shell furnace. Calibration and deconvolution methods were performed according to previous reports.<sup>32</sup>

**2.3. Catalytic Rate and Selectivity Measurements.** Zeolites in their H-form (0.005–0.20 g, sieved to 180–250

 $\mu$ m) were placed within a quartz tube (7 mm I.D.) and supported between quartz wool plugs. The reactor temperature was controlled using a resistively heated three-zone furnace (Applied Test Systems Series 3210) and Watlow controllers (EZ-Zone series). Temperatures were measured with a Type K thermocouple placed at the external surface of the quartz reactor tube at the midpoint of the catalyst bed. The samples were treated in a flowing stream of O<sub>2</sub> (5 kPa) in He (UHP, 99.999%, Indiana Oxygen) or in pure H<sub>2</sub> (UHP, 99.999%, Indiana Oxygen) at 803 K for 2 h (0.0167 K s<sup>-1</sup>) and then cooled to reaction temperature (718-778 K) in a flowing He or H<sub>2</sub> and held for 0.5 h. Propane (10 kPa, 5 kPa Ar, balance He, Indiana Oxygen) and H2 were diluted in He to pressures of 0.6-2.2 and 0-20 kPa, respectively, at volumetric flow rates of 0.4-2.9 cm<sup>3</sup> s<sup>-1</sup> (at STP) and fed to the reactor. Propane conversions were kept below 2% at all conditions to minimize secondary reactions, which become prevalent as alkene pressures increase with increasing alkane conversions. Reactant and product concentrations in the inlet and outlet streams were measured by gas chromatography (HP 6890 Series) using flame ionization detection and a GS-Alumina KCl capillary column for molecular speciation (0.53 mm I.D., Agilent).

Alkene and H<sub>2</sub> co-products were introduced along with alkane reactants by converting a fraction of the propane in the reactant mixture (<1%) on a catalyst bed of H-MFI-17. This pre-bed was placed in a separate reactor and resistively heated furnace (National Element Inc., model FA120, held at temperatures between 718 and 748 K) located upstream of the reactor described above, which contained the zeolite sample (held at 748 K) intended for measurement of propane cracking and dehydrogenation rates. The composition of the effluent stream from the first reactor was quantified by bypassing the second reactor and instead delivering it to the GC. After the effluent from the first reactor containing propane and products (0.5–16 Pa) became invariant in composition, it was delivered to the inlet of the second reactor. Product formation rates on H-MFI-17 or H-MFI-140 in the second reactor were determined by differences in the composition of its influent and effluent streams.

Propene hydrogenation rates were measured by treating H-form zeolites in 101 kPa  $\rm H_2$  at 803 K for 2 h (0.0167 K s<sup>-1</sup>) and cooling under  $\rm H_2$  to 748 K. Propene (1 kPa, 5 kPa Ar, balance He, Indiana Oxygen) and  $\rm H_2$  were diluted in He to 0.03–0.06 and 30–100 kPa, respectively, and molar flow rates were varied to achieve site contact times between 200 and 2000 s (mol H<sup>+</sup>) (mol  $\rm C_3H_6)^{-1}$ . Reactant and product concentrations were quantified using the GC methods reported above for propane dehydrogenation reactions.

## 3. RESULTS AND DISCUSSION

In light of the disparate propane dehydrogenation activation barriers on H-form zeolites reported in the literature, we start in Section 3.1 by describing zeolite pretreatments and reaction conditions that result in the sole involvement of proton sites in propane dehydrogenation turnovers. The kinetic signatures of protolytic alkane pathways become evident from the relative barriers measured for dehydrogenation and cracking and from the strict first-order dependence of turnover rates on propane pressure and the absence of any kinetic inhibition by dehydrogenation products (propene, H<sub>2</sub>). Section 3.2 then shows that H-form zeolites can acquire an extrinsic dehydrogenation site that forms during exposure to propane reactants and/or its alkene products when H<sub>2</sub> is essentially

Table 1. Proton Site and Structural Properties of H-Form Zeolites

			number of H <sup>+</sup> sites			$V_{\mathrm{micro}}^{}} \left(/\mathrm{cm}^{3} \mathrm{~g}^{-1}\right)$
sample <sup>a</sup>	origin	Si/Al <sup>b</sup>	$(/10^{-3} \text{ mol g}^{-1})^c$	(/Al)	$(/unit cell)^d$	
MFI-17	Zeolyst CBV3024E	17	0.66	$0.72^{f}$	3.8	0.15
MFI-43	Zeolyst CBV8014	43	0.32	0.85	1.8	0.14
MFI-140	Zeolyst CBV28014	140	0.12	0.92	0.7	0.14
MOR-10	Zeolyst CBV21A	10	1.51	0.94	4.4	0.19
CHA-16	Di Iorio and Gounder <sup>31</sup>	16	0.96	0.98	2.1	0.21

"Sample nomenclature is XXX-Y. XXX, framework type; Y, Si/Al ratio. Determined by AAS. Uncertainty is  $\pm 10\%$ . Determined by NH<sub>3</sub> TPD. Uncertainty is  $\pm 10\%$ . Based on unit cells containing 96 (MFI), 48 (MOR), or 36 (CHA) T-atoms. Calculated from N<sub>2</sub> (MFI, MOR) and Ar (CHA) adsorption isotherms. H+/Al values less than 1 on H-MFI-17 have been measured independently using in situ pyridine (H+/Al = 0.65) and ex situ NH<sub>3</sub> (H+/Al = 0.52) titrations.

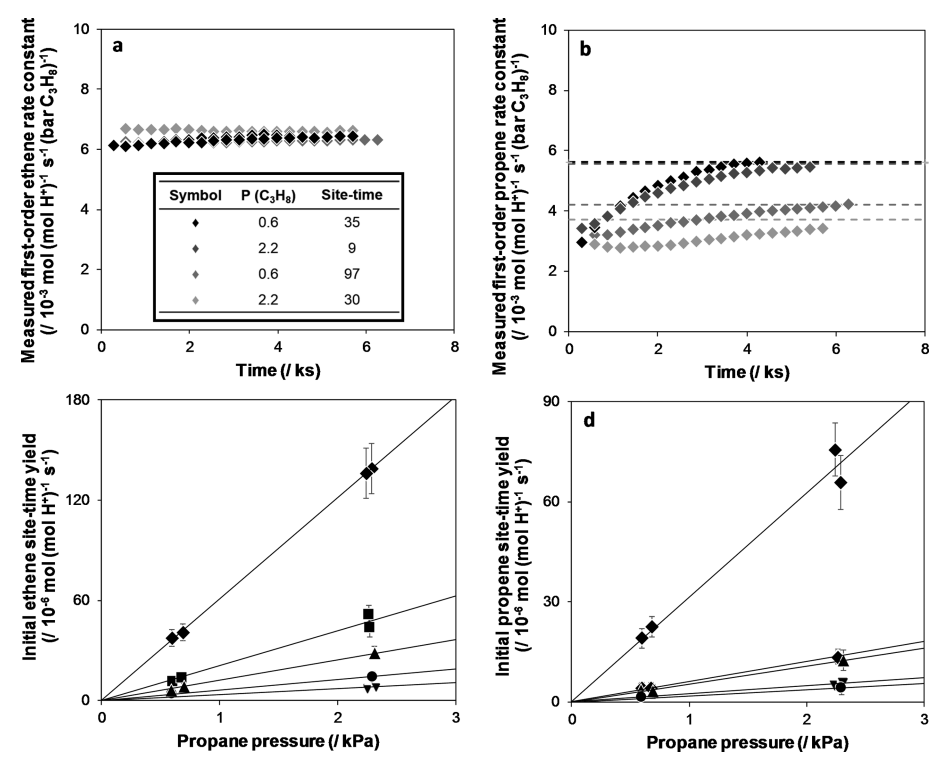


Figure 1. Rate data (748 K) for propane reactions with co-fed  $H_2$  (20 kPa) on H-form zeolites after treatment in  $H_2$  (101 kPa, 803 K, 2 h). Transient changes in first-order rate constants (per H<sup>+</sup>) measured for (a) ethene and (b) propene formation on H-MFI-17 at varying conditions ( $C_3H_8$  pressures (kPa) and site contact times (s (mol H<sup>+</sup>) (mol  $C_3H_8$ )<sup>-1</sup>); see legend in (a)), with dashed lines of different shades of gray to represent steady-state values at each condition in (b). Initial (c) ethene and (d) propene site-time yields (per H<sup>+</sup>) on H-MFI-17 (solid diamond), H-MFI-43 (solid square), H-MFI-140 (solid circle), H-MOR-10 (solid triangle), and H-CHA-16 (solid down triangle); solid lines are regressions of the data to eq 1.

absent. Such extrinsic active sites catalyze propane dehydrogenation at rates with lower barriers than protons, but they are strongly inhibited by dehydrogenation products (propene,  $H_2$ ). These extrinsic sites do not catalyze propane cracking, which occurs solely at protons at all reaction conditions.

Section 3.3 provides evidence that these extrinsic sites consist of unsaturated organic residues that can extract H-atoms from reactant alkanes and then recombine them to desorb  $H_2$ , thus restoring their unsaturation and enabling catalytic turnovers. The formation and reactivity of these carbonaceous deposits can be suppressed by treating H-form zeolites in  $H_2$  instead of oxidizing environments and by introducing high  $H_2$  pressures in inlet streams to avoid forming  $H_2$ -deficient regions within catalyst beds. In Section 3.4, rate measurements without co-fed products are reported on zeolites of different framework topologies and  $H^+$  site densities. These data reveal both the general nature of these phenomena for

microporous solid acids and the increasing prevalence of extrinsic active sites as the density of proton-free voids increases in zeolite samples. Adequate precautions taken to avoid H2-deficient regions within catalyst beds allow measurements of proton-catalyzed monomolecular alkane dehydrogenation uncorrupted by contributions from extrinsic sites, as confirmed in Section 3.5 by measurements of the reverse propene hydrogenation reaction in excess H2 and by treatments based on De Donder relations between chemical affinities for elementary steps and their equilibrium and rate constants. We conclude in Section 3.6 by summarizing the precautions required to isolate the contributions from protoncatalyzed alkane dehydrogenation and by examining the role of extrinsic carbonaceous active sites in causing discrepancies among the previous literature reports of alkane dehydrogenation.

Table 2. Kinetic Parameters for Protolytic Propane Cracking and Dehydrogenation on H-Form Zeolites Measured Here (20 kPa Co-fed H<sub>2</sub>) and Reported by Gounder and Iglesia<sup>9</sup> (No Co-fed H<sub>2</sub>)

		H-MFI-17	H-MFI-43	H-MFI-140	H-MOR-10	H-CHA-16
				Cracking		
$k_{\text{meas,C}} (748 \text{ K})^a$	this work	6.2	1.6	0.6	1.2	0.4
	ref 9	6.3	1.5	n.m. <sup>d</sup>	1.4	n.m. <sup>d</sup>
$E_{\rm meas,C}^{b}$	this work	150	150	164	150	154
	ref 9	155	150	n.m. <sup>d</sup>	160	n.m. <sup>d</sup>
$\Delta S_{\rm meas,C}^{c}$	this work	-94	-104	-95	-109	-112
	ref 9	-88	-106	n.m. <sup>d</sup>	-99	n.m. <sup>d</sup>
				Dehydrogenation		
$k_{\text{meas,D}} (748 \text{ K})^a$	this work	3.3	0.7	0.2	0.5	0.3
	ref 9	3.9	0.8	n.m. <sup>d</sup>	2.2	n.m. <sup>d</sup>
$E_{\rm meas,D}^{b}$	this work	189	193	200	210	189
	ref 9	204	194	n.m. <sup>d</sup>	198	n.m. <sup>d</sup>
$\Delta S_{\mathrm{meas,D}}^{}c}$	this work	-47	-56	-56	-34	-69
,	ref 9	-26	-52	n.m. <sup>d</sup>	-56	n.m. <sup>d</sup>

"Units of (/10<sup>-3</sup> mol (mol H<sup>+</sup>)<sup>-1</sup> s<sup>-1</sup> bar<sup>-1</sup>); uncertainty is  $\pm 15\%$ . "Units of kJ mol<sup>-1</sup>; uncertainty is  $\pm 8$  kJ mol<sup>-1</sup>. "Units of J mol<sup>-1</sup> K<sup>-1</sup>; uncertainty is  $\pm 10$  J mol<sup>-1</sup> K<sup>-1</sup>. "n.m., not measured.

Table 1 summarizes the proton site and structural properties of the zeolites used in this study. Three MFI zeolites and one MOR zeolite were obtained commercially and one CHA zeolite was prepared using reported protocols. X-ray diffraction (XRD) patterns (Figure S1, SI) and micropore volumes calculated from N<sub>2</sub> (77 K; MFI, MOR, Figure S2, SI) and Ar (87 K; CHA, Figure S3, SI) adsorption isotherms confirmed the structure and crystallinity of each topology based on comparisons to the International Zeolite Association (IZA) database. The number of acidic protons from NH<sub>3</sub> evolution during temperature-programmed desorption (TPD) was similar to the number of Al atoms in each sample (H<sup>+</sup>/Al = 0.72–0.98; Table 1), consistent with the predominant presence of Al heteroatoms within silicate frameworks.

**3.1. Transient and Steady-State Rates of Propane Reactions on Acidic Zeolites.** Zeolites in their H-form were treated in flowing  $H_2$  (101 kPa, 803 K, 2 h) and then exposed to propane at different pressures and molar flow rates to vary site contact times (s (mol H<sup>+</sup>) (mol  $C_3H_8$ )<sup>-1</sup>) with  $H_2$  (20 kPa) also present in the inlet stream. Rates of formation of ethene and propene products (per H<sup>+</sup>, 748 K) were measured as a function of time-on-stream. Forward rates of propene formation were determined by rigorously correcting measured rates of propene formation by the approach-to-equilibrium ( $\eta$ ) term; values of  $\eta$  were less than 0.03 at the low propane conversions used here (<1%), even at high inlet  $H_2$  pressures (additional details in Section S4, SI).

Figure 1 shows that on H-MFI-17 (data on all MFI, MOR, and CHA samples in Figures S4–S8, SI), first-order rate constants (mol (mol  $H^+$ )<sup>-1</sup> s<sup>-1</sup> (bar  $C_3H_8$ )<sup>-1</sup>) measured for ethene formation were independent of propane pressure and site contact time at all times-on-stream (Figure 1a), while those for propene formation were so only at the very early stages of reaction (Figure 1b). Measured first-order rate constants for propene formation systematically increased with time-on-stream over a period corresponding to less than one turnover ( $C_3H_6$  formed per  $H^+$ ) and approached a nearly constant value that depended on both the propane pressure and site contact time (Figure 1b).

For all zeolites studied, ethene and propene site-time yields (STYs; product formation rate per  $\mathrm{H}^+$ ) extrapolated to zero cumulative product turnovers (i.e., initial time-on-stream) were

proportional to propane pressure (Figure 1c,d) and independent of site contact time. These data indicate that reaction products do not inhibit cracking or dehydrogenation rates on H-form zeolite samples at these conditions (Figure S9, SI). These initial ethene and propene STYs extrapolate to zero values at zero propane pressure, consistent with cracking and dehydrogenation rates that are strictly proportional to the propane pressure and independent of the concentration of products during the early stages of reaction

$$r_{0,i} = k_{\text{meas},i} P_{C_3 H_8}$$
 (1)

Here,  $r_{0,i}$  is the propane cracking (i=C) or dehydrogenation (i=D) rate extrapolated to zero turnovers,  $k_{\mathrm{meas},i}$  is the corresponding first-order rate constant, and  $P_{\mathrm{C_3H_8}}$  is the propane pressure. The molar ratios of ethene to methane in products were near unity on all samples  $(1.0 \pm 0.1; \mathrm{Figure~S10}, \mathrm{SI})$ . Propene and  $\mathrm{H_2}$  were the only other products detected, indicating the absence of bimolecular alkene-initiated reactions mediated by carbenium ions. These observations are consistent with the prevalence of monomolecular protolytic cracking and dehydrogenation reactions catalyzed by acidic protons, during the early stages of use in catalysis.

First-order rate constants for protolytic propane cracking and dehydrogenation on H-zeolites were determined by regressing the data in Figure 1c,d to the functional form of eq 1. Their values are listed in Table 2 together with those reported on the same samples by Gounder and Iglesia9 at similar conditions (748 K, per H<sup>+</sup>, 0-4 kPa C<sub>3</sub>H<sub>8</sub>) from rates measured at steady state but without H<sub>2</sub> added to inlet streams. Protolytic propane cracking rate constants are similar to those previously reported (±20%) on H-MFI-17, H-MFI-43, and H-MOR-10.9 Protolytic propane dehydrogenation rate constants were also similar on H-MFI-17 and H-MFI-43 in both studies, but were about 4-fold lower on H-MOR-10 in this study (Table 2) than in the previous study. Protolytic propane cracking and dehydrogenation rate constants (per H<sup>+</sup>) also differed among the three MFI samples studied here (Table 2) and among the five MFI samples reported by Gounder and Iglesia. These authors proposed that reactivity differences of protons located in different MFI void environments (straight and sinusoidal channels and their intersections) would result in such turnover rate differences<sup>9</sup> and noted that the earlier

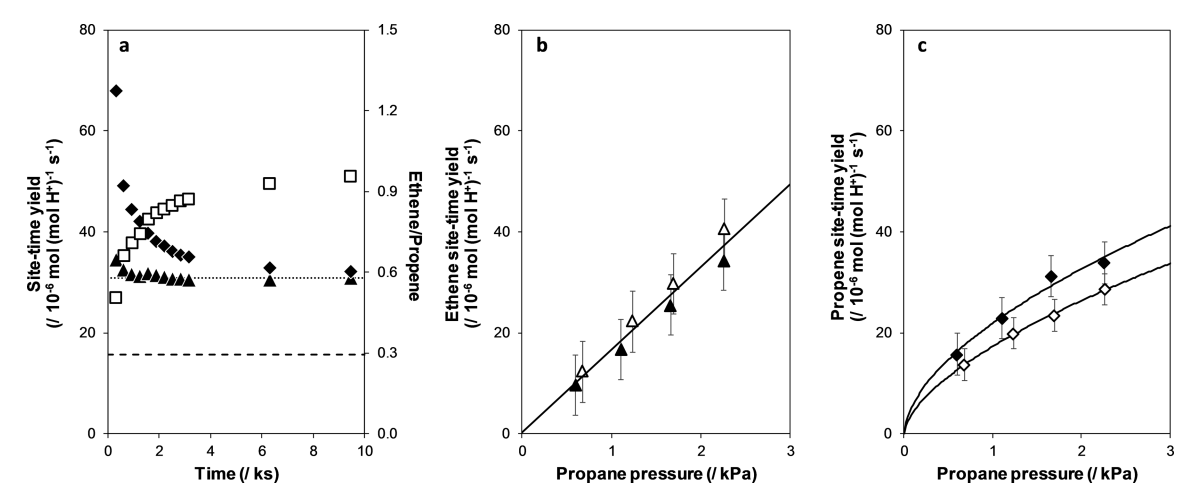


Figure 2. (a) Transient ethene (solid up triangle) and propene (solid diamond) site-time yields (748 K, per H<sup>+</sup>) and ethene/propene ratios (open square) on H-MFI-43 measured at 2.2 kPa  $C_3H_8$  and a residence time of 2 s (mol H<sup>+</sup>) m<sup>-3</sup> following pretreatment in 5 kPa  $O_2$  (803 K, 2 h); expected protolytic cracking (dotted line) and dehydrogenation (dashed line) rates calculated from rate constants in Table 2. Steady-state (b) ethene and (c) propene site-time yields (748 K, per H<sup>+</sup>) measured at different residence times (7 s (mol H<sup>+</sup>) m<sup>-3</sup> (open symbols); 2 s (mol H<sup>+</sup>) m<sup>-3</sup> (closed symbols)). The solid line in (b) represents the regression of data to eq 1, while solid curves in (c) represent the regression of data to a power-law model solely intended to guide the eye.

reports of equivalent *n*-hexane cracking rates (per Al) among MFI zeolites of varying composition by Haag and co-workers<sup>3S</sup> would also be consistent with such location-specific reactivity but for a set of samples in which Al is similarly distributed among T-sites in all samples, a possibility also mentioned by Haag and co-workers.<sup>3S</sup>

Measured activation energies and entropies for protolytic propane cracking and dehydrogenation were calculated from initial propane cracking and dehydrogenation rates on all zeolites between 718 and 778 K, after treatment in H<sub>2</sub> (101 kPa, 803 K, 2 h) and with 20 kPa H<sub>2</sub> present in the inlet stream (Figures S11-S15, SI). As for the rate data at 748 K, ethene and propene STY at 718 and 778 K were first-order in propane pressure (Figure S16, SI) and thus not inhibited by products (Figure S17, SI), because inhibition would have caused STY to increase sub-linearly with propane pressure from the concomitant increase in pressures of its dehydrogenation products. These rate data and those reported by Gounder and Iglesia were used to determine the activation energies (Figure S18, SI) that are summarized in Table 2. Activation energies measured here for protolytic cracking (150-164 kJ mol<sup>-1</sup>; Table 2) are similar to those reported previously on H-zeolites (145-167 kJ mol<sup>-1</sup>), <sup>22-26</sup> and measured dehydrogenation activation energies of 189-210 kJ mol<sup>-1</sup> (Table 2) are about 40 kJ mol<sup>-1</sup> higher than those for protolytic propane cracking.

Measured activation energies for protolytic cracking and dehydrogenation in the first-order kinetic regime reflect the formation energies of their respective carbonium-ion-like transition states from a gaseous reactant molecule and an uncovered proton. The higher barriers for propane dehydrogenation than for cracking (by 25–40 kJ mol<sup>-1</sup>), as measured here and in previous work, reflect the less exothermic proton affinity of C–H than C–C bonds in propane (by 25–40 kJ mol<sup>-1</sup>)<sup>36,37</sup> according to Born–Haber thermochemical cycle analyses 11 (additional details in Section S5, SI). These activation energies for propane dehydrogenation are consistent with the earlier report by Gounder and Iglesia; they are among the highest values reported on H-form zeolites from rate measurements at steady-state using propane as the reactant without added H<sub>2</sub> to inlet streams (67–202 kJ

 $\text{mol}^{-1}$ ).  $^{9,22-26}$  Activation energies for propane cracking measured here are essentially identical to those reported in earlier studies (145-167 kJ mol<sup>-1</sup>). Propane cracking rates remained invariant with time-on-stream (Figure 1a; Figures S4-S8, SI), confirming that proton active sites remain predominantly uncovered and undisturbed during conditions typical of protolytic alkane activation catalysis. Taken together, these observations implicate a distinct non-protonic active site as the genesis of the additional propene observed with increasing time-on-stream during the approach to the catalytic steady state. This second dehydrogenation active site appears to form in situ, as it is not present at zero turnovers on Hzeolite samples pretreated in H<sub>2</sub>. It selectively reacts propane to form propene without concurrent cracking events, via pathways that proceed with much lower barriers and different kinetic behavior than protons, as discussed in the next section.

3.2. Product Inhibition by Dihydrogen and Propene at Reaction-Derived Active Sites. Propene formation rates (748 K, per H<sup>+</sup>) on H-form zeolites measured with 20 kPa H<sub>2</sub> in the inlet stream increased with time-on-stream and approached constant values (Figure 1b; Figures S4-S8, SI). These steady-state values depend on the specific propane pressure and site contact time (or residence time) of each experiment. Asymptotic rates are lower for experiments at longer bed residence times and higher propane pressures, both of which lead to higher propane conversion and thus to higher product pressures (Figure S19, SI). The number of dehydrogenation turnovers (defined as cumulative C<sub>3</sub>H<sub>6</sub> formed per H+) required to attain steady-state propene formation rates at each condition was below unity (0-0.6 per H<sup>+</sup>; Figures S4-S8, Supporting Information), suggesting that the transient approach to steady state is unrelated to dehydrogenation turnovers at H<sup>+</sup> sites.

The inhibition of propene formation rates by  $H_2$  and alkene products was confirmed by co-feeding reaction products. These products were formed on a bed of H-form zeolite (H-MFI-17) that was placed before a subsequent reactor that contained the zeolite sample (either H-MFI-17 or H-MFI-140) used for measurement of reaction rates. This pre-reactor was used to convert a small percentage ( $\sim$ 1%) of the inlet molar

rate of propane to its cracking and dehydrogenation products before its effluent stream entered the second bed. As the prebed temperature was increased (718-748 K) to increase the propene and H2 pressures entering the second bed (kept at 748 K), propene formation rates measured on the sample in the second bed decreased and ultimately became insensitive to  $H_2$  and  $C_3H_6$  product pressures above  $\sim$ 2 Pa of each product; in contrast, ethene formation rates were unaffected by the presence or pressure of dehydrogenation products (Figure S20, SI). At H<sub>2</sub> and C<sub>3</sub>H<sub>6</sub> pressures above 2 Pa, propane cracking and dehydrogenation rates were similar to those extrapolated to zero turnovers when samples were pretreated in H2 and when H<sub>2</sub> was present in the inlet stream (Figure S20, SI). These results indicate that propene and H2 inhibit dehydrogenation rates on the extrinsic active site, even at the very low product pressures of purportedly differential conditions. These observations serve as a useful reminder that reaction rates, and thus the concentrations of any species that determine such rates, must remain essentially invariant (i.e., gradientless) throughout a catalytic packed bed to ensure differential conditions, which are not guaranteed solely by low reactant conversions.

The transient evolution of propane cracking and dehydrogenation rates was also monitored in the absence of dehydrogenation products in the inlet stream after treating H-form zeolites in O<sub>2</sub>-containing streams (5 kPa O<sub>2</sub> in balance He, 803 K) instead of pure H<sub>2</sub> streams (803 K). Treatments with O2-containing streams are commonly used in attempts to remove adventitious organic residues from zeolites before rate measurements. 9,22-26 Ethene and propene formation rates (per H<sup>+</sup>) are shown in Figure 2a on H-MFI-43 as a function of time-on-stream (data on all samples in Figure S21, SI). Ethene formation rates (per H<sup>+</sup>) remained constant with time-onstream and were similar to those measured in the presence of co-fed H<sub>2</sub> (Figure 2a, dotted line). In contrast, propene formation rates (per H<sup>+</sup>) decreased about 2-fold before reaching constant values (Figure 2a). Both initial and steadystate propene formation rates (per H<sup>+</sup>) were higher than the protolytic dehydrogenation rate (Figure 2a, dashed line) determined from measured rates extrapolated to zero turnovers with H<sub>2</sub>-containing inlet streams (Figure 1b; Figures S4-S8,

After attaining constant propene formation rates on each sample, increasing or decreasing the residence time led to additional transients that decreased or increased the steadystate propene formation rates, respectively (Figure S22, SI). Ethene formation rates, however, remained unchanged throughout these experiments (Figure S22, SI). In the absence of co-fed products, these constant ethene formation rates were proportional to propane pressure and unaffected by residence time (Figure 2b), but those for propene formation increased sub-linearly with propane pressure and decreased as the residence time and the prevalent product pressures increased (Figure 2c). As a result, first-order propene formation rate constants on H-form zeolites measured in the absence of cofed products systematically decreased when propene (and H<sub>2</sub>) pressures increased as a result of higher propane reactant pressures and longer residence times (Figure S23, SI). These data are consistent with the inhibition of the extrinsic active site by dehydrogenation products, as also observed during deliberate co-feeding of dehydrogenation products (Figure S20, SI).

The monotonic decrease in measured first-order propene formation rate constants with increasing propene and H<sub>2</sub> pressure was not evident on all samples (Figure S23, SI), suggesting that back-mixing of partially converted reactant streams led to higher propene pressures at the beginning of catalyst beds in certain cases. The relatively short beds (the ratio of the bed length to the aggregate diameter <20) used in these experiments led to significant axial mixing. The relative rates of convection and axial dispersion were similar in these cases, leading to Péclet numbers of order 1<sup>38</sup> (Section S9, SI). Smaller Péclet numbers cause inhibiting products to disperse more readily to earlier axial positions along the bed, thus enhancing their inhibitory effects. As a result, measured propene formation rates at a given residence time are different for beds of proportionately different lengths and linear fluid velocities. Propene formation rates collected at lower Péclet numbers more closely resemble protolytic dehydrogenation rates because these conditions approach well-mixed reactors that remove axial gradients in product pressures, thus more strongly inhibiting the extrinsic dehydrogenation function (Figure S24, SI). Taken together, these data indicate that products of propane dehydrogenation (propene, H<sub>2</sub>) inhibit propene formation events on a second active site that is unrelated to Brønsted acidic protons and that forms during the reaction. These observations also illustrate how conditions typically used in lab-scale reactors can conflate kinetic and hydrodynamic effects of reactant pressure and residence time. This represents a disconcerting conclusion given that literature reports seldom consider such matters when measuring the data of purported kinetic origin or document the required details when describing the methods used to collect catalytic data, thus preventing independent replication or retroactive interpretation of rate data.

3.3. Effects of H<sub>2</sub> on the Removal of Reaction-Derived Organic Residues Acting as an Extrinsic Dehydrogenation Function. These results clearly point to reactionderived organic residues as an extrinsic function for dehydrogenation via hydrogen transfer. Such residues may form via reactions of alkene products (e.g., oligomerization, cyclization, hydride transfer)<sup>39</sup> or from unsaturated impurities in reaction mixtures (e.g., propyne, 1,3-butadiene), but they can be scavenged or rendered inactive by reactions with H<sub>2</sub>. The presence of adventitious unsaturated feed impurities in our studies was ruled out by the addition of H<sub>2</sub> (20 kPa) to reactant streams and the placement of a Pt/SiO<sub>2</sub> catalyst (293 K) upstream of the zeolite bed to hydrogenate any trace unsaturated impurities (details in Section S10, SI). Such protocols did not have any detectable effect on measured propene formation rates on H-MFI-43 (Figure S25, SI).

The purposeful deposition of carbonaceous structures on H-form zeolites typically involves exposure to unsaturated hydrocarbons, such as propene, at high temperatures ( $\sim$ 1000 K); the formation of non-volatile organic residues was evident by dissolving the zeolite in HF and detecting the zeolite-templated carbonaceous deposits formed (ZTC). Organic residues formed on H-FAU zeolites during reactions of benzene (773–1073 K) in an inert He environment contained H/C ratios consistent with fused aromatic rings. In these studies, H<sub>2</sub> inhibited the formation of carbonaceous deposits (1–5 MPa H<sub>2</sub>), purportedly because benzene and other intermediates were hydrogenated at H<sup>+</sup> sites to form volatile products. Similar H<sub>2</sub> co-feed strategies have been used to mitigate the formation of unsaturated organic residues during

 $n\text{-}\mathrm{C}_7$  cracking (543 K, 0–2 MPa  $\mathrm{H}_2)^{43}$  and methanol-to-hydrocarbon conversion (623 K, 1.6 MPa  $\mathrm{H}_2)^{44}$  on H-MFI zeolites. Exposing carbonaceous deposits to  $\mathrm{H}_2$  leads to the formation of  $\mathrm{CH}_4^{45,46}$  via hydrogenation reactions that first remove the methyl groups from substituted aromatics (e.g., toluene, diphenylmethane) and then lead to aromatic ring saturation and C–C bond cleavage to form  $\mathrm{C}_1\mathrm{-}\mathrm{C}_2$  hydrocarbons. Thus,  $\mathrm{H}_2$  allows the scavenging and hydrogenation of unsaturated organic residues that form during acid-catalyzed reactions on zeolites.

These previous observations, taken together with the effects of product concentrations and chemical treatments on the contributions from extrinsic dehydrogenation sites, led us to explore more direct probes of the presence and involvement of organic residues as an extrinsic catalytic dehydrogenation function. Figure 3a shows the results of an experiment in which

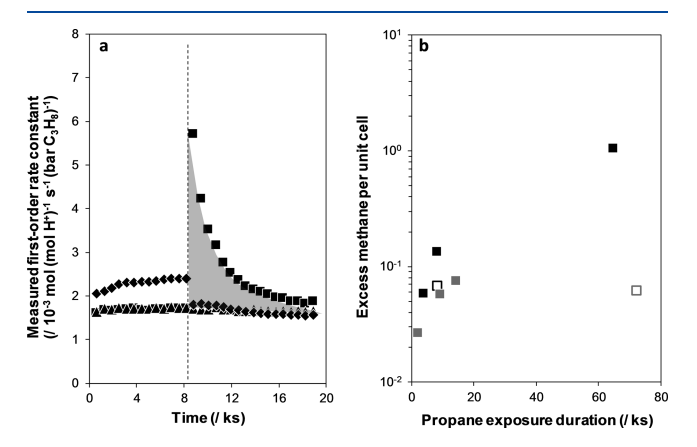


Figure 3. (a) Measured rate constants of methane (solid square), ethene (solid triangle), and propene (solid diamond) formation (per H<sup>+</sup>, 748 K) on H-MFI-43 (0.6 kPa  $C_3H_8$ , 17 s (mol H<sup>+</sup>) m<sup>-3</sup>, 2.5 ×  $10^{-3}$  m bed height). The dashed line at ~8 ks indicates a step-change increase in co-fed  $H_2$  from 0 to 20 kPa. The gray shaded region represents the excess methane formed. (b) Excess methane removed per unit cell (96 T-atoms) from H-MFI-43 during exposure to propane (748 K) after a step-change increase in co-fed  $H_2$  (0–20 kPa). Experiments performed under 0.6 kPa (solid square) or 2.2 kPa (gray box solid)  $C_3H_8$  and with catalyst bed heights of 2.5 ×  $10^{-3}$  (closed) and  $7.5 \times 10^{-3}$  m (open) of H-MFI-43.

H-MFI-43 was first treated in H<sub>2</sub> (20 kPa, 803 K) and then exposed to propane (0.6 kPa C<sub>3</sub>H<sub>8</sub> in He, 748 K) without cofed H<sub>2</sub> until constant propene formation rate constants were achieved (~8 ks); these conditions also led to the formation of the equimolar CH<sub>4</sub>/C<sub>2</sub>H<sub>4</sub> mixtures expected from protolytic cracking. Then, H<sub>2</sub> (20 kPa) was added to the reactant stream without any changes in propane pressure or residence time. Propene formation rate constants decreased immediately upon co-feeding H<sub>2</sub> (from 2.5 to  $1.9 \times 10^{-3}$  mol (mol H<sup>+</sup>)<sup>-1</sup> s<sup>-1</sup> (bar  $C_3H_8)^{-1}$ ; Figure 3a) and then more gradually with time over ~5 ks to reach values  $(1.7 \times 10^{-3} \text{ mol (mol H}^+)^{-1} \text{ s}^{-1} \text{ (bar }$ C<sub>3</sub>H<sub>8</sub>)<sup>-1</sup>; Figure 3a) that were similar to steady-state values measured with 20 kPa H<sub>2</sub> co-feeds (Figure S5d, SI); in contrast, ethene formation rate constants were unaffected by H<sub>2</sub> co-feeds and did not vary with time. These data show that H<sub>2</sub> inhibits an extrinsic function that mediates only dehydrogenation events and which is not associated in its formation or function with the protons that mediate protolytic cracking reactions.

CH<sub>4</sub> formation rate constants, however, increased sharply upon  $H_2$  introduction (from 1.7 to 5.8 × 10<sup>-3</sup> mol (mol H<sup>+</sup>)<sup>-1</sup>  $s^{-1}$  (bar  $C_3H_8$ )<sup>-1</sup>; Figure 3a) and then decreased with time to the same constant value obtained before H2 introduction, at which point it formed the equimolar CH<sub>4</sub>/C<sub>2</sub>H<sub>4</sub> ratios expected from protolytic cracking. Similar experiments on H-MFI-43 samples that attained constant rates after exposure to propane at different pressures (0.6 or 2.2 kPa C<sub>3</sub>H<sub>8</sub>) and for different time-on-stream (2-75 ks) using packed beds of different heights (2.5 or 7.5 mm; Figures S26 and S27, SI; data on H-MOR-10 in Figure S28, SI) also led to the evolution of excess CH<sub>4</sub> (other saturated products, such as ethane, were not detected). The formation of excess amounts of CH<sub>4</sub> upon H<sub>2</sub> introduction indicates that H2 leads to the removal of some or all reaction-derived organic residues deposited during reactions in the absence of H<sub>2.</sub>

The excess amount of CH<sub>4</sub> formed upon H<sub>2</sub> introduction on H-MFI-43 (Figure 3a, gray shaded region) was 0.14 CH<sub>4</sub> per zeolite unit cell  $(2.3 \times 10^{-5} \text{ mol CH}_4 \text{ g}^{-1})$ . Figure 3b shows the amount of excess CH4 formed (per unit cell) at various propane exposure times and propane pressures before introducing H2 to inlet streams and on catalyst beds of different heights. Longer beds (7.5 mm) formed smaller amounts of excess CH<sub>4</sub> (0.07 vs 0.13 CH<sub>4</sub> per unit cell) than shorter beds (2.5 mm) after exposure to 0.6 kPa C<sub>3</sub>H<sub>8</sub> for 8 ks at the same gas linear velocity  $(2.6 \times 10^{-2} \text{ m s}^{-1})$ , indicating that carbon deposition does not occur uniformly throughout catalyst beds. The formation of smaller amounts of excess CH<sub>4</sub> (per unit cell) on longer beds is consistent with the reactor hydrodynamics characteristic of Péclet numbers of order  $\sim 10^{0}-10^{1}$ , which preserve H<sub>2</sub>-deficient regions near the bed inlet; such H2-deficient regions therefore represent smaller fractions of the packed beds for longer beds. As a result, the deposition of carbonaceous residues occurs chromatographically at the front of catalyst beds where H2-deficient regions prevail, similar to the axial gradients in coke content reported along the H-FAU catalyst beds during propene reactions (723 K, 10 kPa  $C_3H_6$ ).

Smaller amounts of CH<sub>4</sub> were evolved in analogous experiments performed at higher C<sub>3</sub>H<sub>8</sub> pressures (2.2 kPa) but identical bed length and linear velocity (Figure 3b), because the higher product H<sub>2</sub> pressures generated in situ led to the more efficient hydrogenation of unsaturated intermediates, thus mitigating the formation of carbonaceous residues. After each constant propene formation rate was attained for each C<sub>3</sub>H<sub>8</sub>/H<sub>2</sub> reactant mixture, a subsequent switch to pure H<sub>2</sub> also led to the transient evolution of excess CH<sub>4</sub> (Figure S29, SI), albeit a significantly smaller amount (by 3 orders of magnitude) than was removed when C<sub>3</sub>H<sub>8</sub>/H<sub>2</sub> replaced C<sub>3</sub>H<sub>8</sub>/He reactants. The evolution of excess CH<sub>4</sub> in these experiments shows that minority amounts of organic residues are replenished from alkane reactants and thus still present on H-form zeolite surfaces even when H<sub>2</sub> is introduced in inlet streams and that such residues were only fully removed when propane was removed from inlet streams.

These experiments cannot directly discern the specific nature of the reaction-derived extrinsic function for dehydrogenation via hydrogen transfer. Any inquiries about their structure would require fast quenching protocols that are certain to change their composition and H-content. It is evident, however, that their removal by  $\rm H_2$  as  $\rm CH_4$  decreases the rates of propene formation without detectable changes in the rates of ethene formation, via a reaction that occurs

exclusively at proton sites. In fact, carbonaceous deposits have been implicated as active structures in non-oxidative dehydrogenation on  $VO_x/Al_2O_3$  (e.g., ethylbenzene, <sup>50,51</sup> butane, <sup>52</sup> and cyclohexene <sup>53</sup>), and the edges of these carbonaceous deposits have been proposed as plausible active sites for alkane dehydrogenation. <sup>50</sup> A plausible route for these dehydrogenation events is shown in Scheme 1 and includes

Scheme 1. Plausible Prototypical Route for Propane Dehydrogenation via Hydrogen Transfer at a Carbonaceous Deposit (of Arbitrary Structure) That Can Subsequently Desorb H-Atoms as  $\rm H_2$  to Complete a Dehydrogenation Turnover

hydrogen transfer from propane to an unsaturated residue to form a bound propyl radical or hydride transfer to form a bound propoxide, which would then undergo  $\beta$ -hydrogen abstraction to eliminate propene. The hydrogenated form of these carbonaceous residues would then dehydrogenate to desorb  $H_2$  to complete a turnover, restoring its unsaturation and thus its catalytic function. Similar observations of hydrogen transfer between alkanes, alkenes, and carbonaceous intermediates have been recognized during n-hexane cracking on FAU zeolites (723 K) evidenced by concomitant changes in H/C ratios of reaction products and coke content, <sup>54</sup> albeit at

higher conversions (4-20%) than those used in this work (<1%).

The extrinsic nature and reaction-derived origins of these nonprotonic dehydrogenation sites are evident from their negligible contributions during the earliest stages of exposure of H-form zeolites to propane. The transient evolution of propene formation rates appears to reflect concomitant changes in the amount and composition of these organic residues with time, in response to the prevalent chemical potentials of carbon and hydrogen in the reacting mixtures. Such changes influence, in turn, their ability to affect hydrogen transfer reactions from alkanes and the desorption of H-atoms as the  $\rm H_2$  co-products.

The gradual evolution of propene formation rates on H-MFI-43 after different treatments in O2 (5 kPa) and H2 (10 kPa) is shown in Figure 4. An O<sub>2</sub> treatment (803 K, 2 h; Figure 4a) led to propene formation rate constants (748 K) that decreased about 2-fold (from 3.0 to  $1.7 \times 10^{-3}$  mol (mol H<sup>+</sup>)<sup>-1</sup> s<sup>-1</sup> (bar C<sub>3</sub>H<sub>8</sub>)<sup>-1</sup>) and reached constant values after about 3 ks. A subsequent O2 treatment (and He flush for 0.5 h at 748 K) followed by the reintroduction of propane reactants led to a lower initial rate constant  $(2.1 \times 10^{-3} \text{ mol (mol H}^+)^{-1}$  $s^{-1}$  (bar  $C_3H_8$ )<sup>-1</sup>) and to a shorter transient (~0.5 ks) approach to steady-state values, which were similar to those attained before this second O2 treatment (Figure 4b). After these two successive O2 treatments, H-MFI-43 was treated in H<sub>2</sub> (803 K, 2 h) and then flushed with He (748 K, 0.5 h) before reintroducing propane reactants (Figure 4c). The transient evolution of propene formation rates resembled that measured after the first O<sub>2</sub> treatment (Figure 4a), with the propene formation rate constants decreasing (from 3.0 to 1.7 ×  $10^{-3}$  mol (mol H<sup>+</sup>)<sup>-1</sup> s<sup>-1</sup> (bar C<sub>3</sub>H<sub>8</sub>)<sup>-1</sup>) over a similar transient period (~3 ks) as after the initial O<sub>2</sub> treatment. These data indicate that O2 treatments do not fully remove the organic residues that form on H-form zeolites during propane reactions in the absence of co-fed H2; in contrast, H2 treatments at 803 K for 2 h are able to remove them (Figure 3; Figures S26 and S27, SI) and to restore H-MFI-43 to its state before exposure to propane at reaction conditions.

Once steady-state propene formation rates have been attained, subsequent transients in propene formation rates

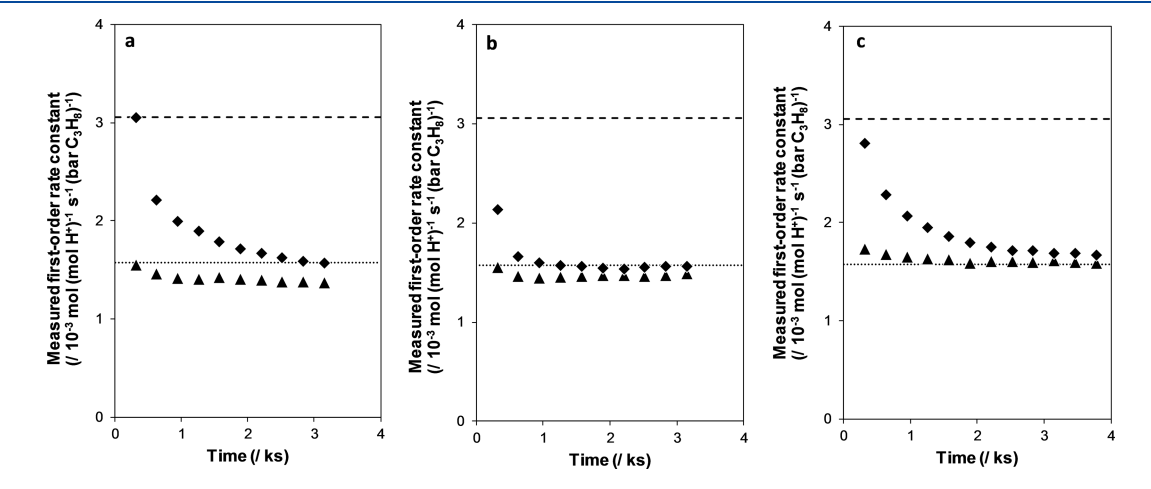
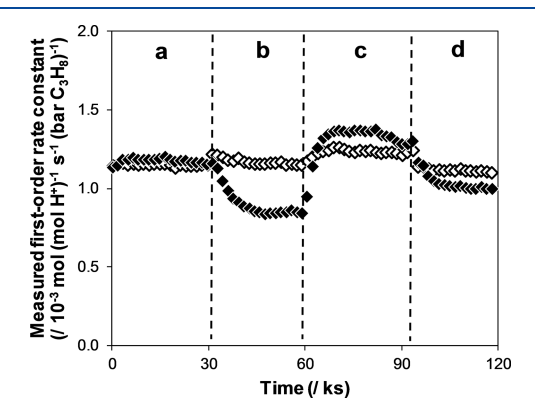


Figure 4. Transients in measured first-order ethene (solid triangle) and propene (solid diamond) formation rate constants (748 K, per H $^+$ ) on H-MFI-43 following (a) first treatment in 5 kPa O $_2$ /He (803 K, 2 h) and He purge (748 K, 0.5 h), (b) second treatment in 5 kPa O $_2$ /He (803 K, 2 h) and He purge (748 K, 0.5 h). The dashed line represents the initial propene formation rate constant after the first O $_2$  treatment, and the dotted line represents the steady-state propene formation rate constant.

are observed when inlet flow rates are changed to vary the bed residence times. This is shown in Figure 5 (data collected on



**Figure 5.** Measured first-order ethene (open diamond) and propene (solid diamond) formation rate constants (748 K, per  $H^+$ ) on H-MOR-10 as a function of time-on-stream, and their response to changes in reactant site contact time (s (mol  $H^+$ ) (mol  $C_3H_8$ )<sup>-1</sup>) corresponding to (a) 43, (b) 99, (c) 29, and (d) 54.

H-MOR-10) for rates measured in the absence of co-fed products. Step changes that increased or decreased the residence times led to a gradual decrease or increase, respectively, in propene formation rate constants (748 K) over 10-20 ks (Figure 5); in contrast, ethene formation rate constants remained constant with time and unaffected by the residence time. Changes to inlet flow rates cause changes to bed residence time and in turn to product pressures, which influence prevalent carbon and hydrogen chemical potentials in reacting mixtures. Such changes also influence linear fluid velocities and thus Péclet numbers, leading to different extents of back-mixing and to differences in the prevalent axial gradients of carbon and hydrogen chemical potentials. These different carbon and hydrogen chemical potentials would cause organic residues to evolve in composition, thus influencing their ability to catalyze dehydrogenation turnovers.

We conclude that the transient evolution in propene formation rates observed upon changes in residence time (Figure 5) reflects such a compositional evolution of these unsaturated surface organic residues; they retain a memory of the hydrogen and carbon chemical potential history from the previous steady state and change their composition with time in response to new hydrogen and carbon chemical potentials in the reacting mixture. The inhibition of propene formation turnovers by products on these carbonaceous active sites cannot arise from the strong adsorption of products (alkenes, H<sub>2</sub>), which would have resulted in much faster changes in propene formation rate constants in response to changes in residence time. Such inhibition reflects instead changes in the reactivity of carbonaceous active sites in response to the effective hydrogen and carbon chemical potentials. Sufficiently high chemical potentials of hydrogen relative to carbon would increase the degree of saturation in organic residues that would limit their ability to abstract H-atoms from reactant alkanes, and sufficiently low hydrogen chemical potentials would increase the degree of unsaturation in organic residues that would limit their ability to desorb H<sub>2</sub>.

These data clearly demonstrate that the initial transient propene formation rates when acidic zeolites are contacted with H<sub>2</sub>-free propane reactants reflect the formation of unsaturated organic residues; they also show that such extrinsic

sites vary in number and/or reactivity in response to the reaction environment. Changes in bed residence time and the resulting changes in the prevalent H<sub>2</sub> and propene concentrations influence dehydrogenation rates (Figure 5; Figure S22, SI) through changes in the number and the H-content (and thus the reactivity) of the organic residues that act as the extrinsic dehydrogenation function. These parallel pathways, catalyzed by intrinsic (protons) and extrinsic (organic residues) functions, contribute in an additive manner to measured propene formation rates, while cracking occurs exclusively on protons. Their relative contributions depend on the reaction environment, on the history of use for each sample, and even on axial dispersion effects; these dispersion effects depend sensitively on details such as bed length, aggregate size, and linear fluid velocities that are seldom considered, controlled, or reported as part of the protocols used to measure catalytic data.

Measured dehydrogenation barriers reflect additive contributions from two functions with very different kinetic parameters and disparate sensitivities to product concentrations, even under nominally "differential" conditions. Not surprisingly, the resulting inconsistent reports of dehydrogenation rates and activation barriers have brought forth widespread confusion and significant discord, and myriad hypotheses about their origins. Next, we illustrate some of the ubiquitous pitfalls inherent in rate measurements at conditions typically used to determine the rates and kinetic parameters for monomolecular dehydrogenation and cracking on H-form zeolites. <sup>9,22–26</sup>

**3.4.** Monomolecular Dehydrogenation Barriers and Corruptions Induced by Extrinsic Reaction-Derived Active Sites. Measured activation barriers for propane cracking (150–164 kJ mol $^{-1}$ ; Table 2) and dehydrogenation (189–210 kJ mol $^{-1}$ ; Table 2) obtained from initial rates on zeolites in their H-form pretreated in  $\rm H_2$  and with  $\rm H_2$  present in the inlet stream are consistent with protolytic pathways at  $\rm H^+$  sites, given that carbonium-ion-like transition states for these parallel pathways differ in energy in a manner proportional to the difference in the ensemble-averaged proton affinity of the C–C and C–H bonds in gaseous propane (25–40 kJ mol $^{-1}$ ).  $^{36,37}$  Such  $\rm H_2$  pretreatments and the presence of added  $\rm H_2$  represent atypical situations in the practice of protolytic alkane activation.  $^{9,22-26}$ 

Figure 6 shows steady-state ethene and propene formation rates on H-form zeolites (without co-fed products) in the semi-logarithmic form appropriate for Arrhenius-type rate dependences. The corresponding activation energies and entropies are reported in Table 3. Measured cracking activation energies (153-169 kJ mol<sup>-1</sup>; Table 3) are similar to those previously attributed to protolytic cracking (150-164 kJ mol<sup>-1</sup>; Table 2) on the four most Al-dense samples (H-MFI-17, H-MFI-43, H-MOR-10, H-CHA-16). Measured cracking activation energies were lower on the most Al-dilute sample (H-MFI-140, 143 kJ mol<sup>-1</sup>; Table 3) that contains the highest density of H+-free voids (Table 1) and thus extrinsic carbonaceous deposits, which appear to generate minority amounts of ethene that become detectable when proton sites are essentially absent. In contrast, dehydrogenation activation energies differed significantly among these samples (67-214 kJ mol<sup>-1</sup>; Table 3), with some zeolites exhibiting deviations from Arrhenius-type behavior (Figure 6), in line with the literature discord about measured dehydrogenation barriers on H-form zeolites  $(65-202 \text{ kJ mol}^{-1})$ .  $^{9,22-26}$ 

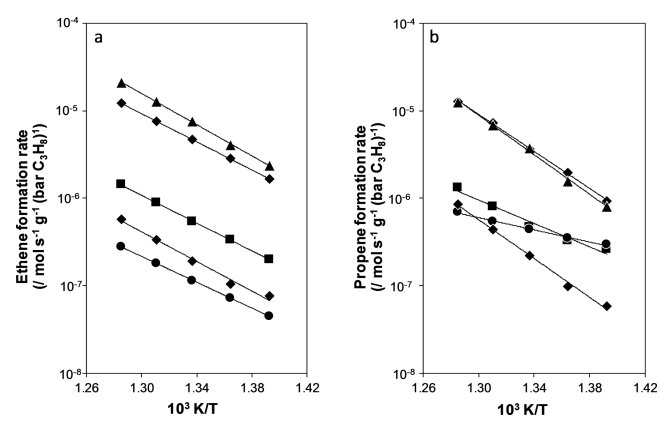


**Figure 6.** Arrhenius plots for steady-state (a) ethene and (b) propene formation rates on H-MFI-17 (solid diamond), H-MFI-43 (solid square), H-MFI-140 (solid circle), H-MOR-10 (solid up triangle), and H-CHA-16 (solid down triangle). Rates are collected from 718 to 778 K at propane pressures of 0.6–2.2 kPa.

On all samples (except H-MFI-140), the measured activation entropies for propane cracking (-103 to -82 J mol<sup>-1</sup> K<sup>-1</sup>) are similar to the values reported previously for propane cracking on H-form zeolites by Gounder and Iglesia  $(-109 \text{ to } -89 \text{ J mol}^{-1} \text{ K}^{-1}).^9$  Propane adsorption at protons present within MFI voids results in significant entropy losses  $(-102 \text{ to } -82 \text{ J mol}^{-1} \text{ K}^{-1})$ , as estimated by the experiment using microcalorimetry and gravimetry  $^{55,56}$  and as also calculated using statistical mechanics treatments for mobile adsorbates (-100 to -70 J mol<sup>-1</sup> K<sup>-1</sup>). See Entropic gains are negligible when adsorbed propane subsequently forms its cracking transition state, according to statistical mechanics estimates of the entropy associated with the one-dimensional rotational degrees of freedom about the C-C bond being cleaved in propane that is accessed by product C1 and C2 molecular fragments in the (C-C-H)+ carbonium-ion-like transition state. 11 These net changes in entropy upon propane adsorption and subsequent formation of the relevant cracking transition state are consistent with the measured activation entropies of about -100 J mol<sup>-1</sup> K<sup>-1</sup> (Table 3).

Carbonium-ion-like transition states for propane dehydrogenation occur later along their reaction coordinates than for propane cracking and are more loosely bound and product-like. Consequently, protolytic dehydrogenation activation entropies are less negative than for cracking. Indeed, the measured activation entropies for dehydrogenation (–35 to –26 J mol<sup>-1</sup> K<sup>-1</sup>; Table 3) are less negative than for cracking on all samples that showed higher measured barriers for dehydrogenation than for cracking (H-MFI-17, H-MOR-10, H-CHA-16; Table 3), as expected from the exclusive

involvement of protolytic alkane activation in such samples. In contrast, the measured dehydrogenation activation entropies (-140 to -210 J mol $^{-1}$  K $^{-1}$ ) are significantly more negative than for cracking on samples (H-MFI-43, H-MFI-140; Table 3) that also showed dehydrogenation barriers much lower than expected for protolytic reactions at H $^+$  sites. Such aberrantly low values of measured dehydrogenation activation entropies have been noted previously $^{26}$  and serve to diagnose the presence of non-protonic functions and reflect both the incorrect normalization of dehydrogenation rates by proton sites and the non-carbonium-ion-like nature of the transition states.

These data show that the evolution of the reaction-derived extrinsic active sites in number and composition influences dehydrogenation rates and their temperature dependence; such extrinsic sites lead to significant contributions to measured rates, which tend to obscure the contributions from monomolecular proton-catalyzed events and to do so to different extents with changes in the reaction temperature. Such effects account for the prevalent literature discord, but contributions from extrinsic sites cannot be retroactively extracted from such data because the number and structure of extrinsic sites depend on the reaction environment (temperature, reactant, and product concentrations), on the temporal and thermal history of the samples, and even on how axial mixing effects influence product concentrations along the catalyst bed. These are important details that are seldom reported with the detail required for such a forensic analysis.

Measured dehydrogenation activation energies and entropies (Table 3) from steady-state rate data also systematically decrease with increasing Si/Al ratio on H-MFI zeolites. Measured barriers on H-MFI-17, H-MOR-10, and H-CHA-16 were similar with  $\rm H_2$  co-feeds (189–210 kJ mol<sup>-1</sup>, Table 2) and without  $\rm H_2$  co-feeds (202–214 kJ mol<sup>-1</sup>). In contrast, the measured barriers on H-MFI-43 and H-MFI-140 were lower without co-fed products (67–125 kJ mol<sup>-1</sup>) than with  $\rm H_2$  co-feeds at initial time-on-stream (193–200 kJ mol<sup>-1</sup>), which are conditions that suppress the extrinsic functions. These data indicate that the contributions from extrinsic reaction-derived active functions to dehydrogenation rates increase proportionally with the fraction of siliceous regions within zeolites and become essentially undetectable on proton-dense zeolites (Si/Al of ~10–16; Table 3).

3.5. Measurements of Propene Hydrogenation Barriers at H<sup>+</sup> Sites and Predictions of Protolytic Dehydrogenation Barriers from De Donder Relations. The rate constants for stoichiometric chemical reactions in their forward and reverse directions, when measured under different reaction conditions that lie far away from equilibrium on either side, are related by the equilibrium constant for the

Table 3. Measured Activation Energies and Entropies for Steady-State Propane Cracking and Dehydrogenation Measured without Co-fed Products on H-Form Zeolites

	H-MFI-17	H-MFI-43	H-MFI-140	H-MOR-10	H-CHA-16			
			Cracking					
$E_{ m meas,C}^{a}$	154	153	143	169	164			
$\Delta S_{ m meas,C}{}^{m b}$	-89	-100	-122	-82	-103			
	Dehydrogenation							
$E_{ m meas,D}^{a}$	202	125	67	208	214			
$\Delta S_{ m meas,D}^{b}$	-27	-140	-210	-26	-35			

<sup>&</sup>lt;sup>a</sup>Units of kJ mol<sup>-1</sup>; uncertainty is ±8 kJ mol<sup>-1</sup>. <sup>b</sup>Units of J mol<sup>-1</sup> K<sup>-1</sup>; uncertainty is ±10 J mol<sup>-1</sup> K<sup>-1</sup>.

overall reaction, for systems in which sites are predominantly bare and the same kinetically relevant step prevails in both directions; such requirements are met for protolytic propane dehydrogenation and propene hydrogenation rates on H-form zeolites.<sup>58</sup>

Propene hydrogenation rates (748 K, per H<sup>+</sup>) measured at high H<sub>2</sub> pressures (>60 kPa) and large H<sub>2</sub>/C<sub>3</sub>H<sub>6</sub> molar ratios (>1000) reflect exclusive contributions from proton-catalyzed pathways because contributions from extrinsic active sites for dehydrogenation (and for its reverse hydrogenation) are suppressed by H<sub>2</sub>. Together with reversibility treatments based on De Donder relations between chemical affinities for elementary steps and their equilibrium and rate constants, <sup>58</sup> propene hydrogenation rates can be used to confirm that propane dehydrogenation rates measured at the conditions of the experiments reported in Section 3.1 indeed solely reflect proton-catalyzed contributions and the high activation barriers characteristic of such routes.

Measured propene hydrogenation rates (748 K, per H<sup>+</sup>) increased linearly with both  $C_3H_6$  and  $H_2$  pressures on H-form zeolites (Figure S30, SI), consistent with the previous reports at similar conditions (748 K, 1–4 kPa  $C_3H_6$ , 10–100 kPa  $H_2$ ). Such kinetic behavior indicates that protons remain essentially bare at the conditions of catalysis, leading to the rate equation

$$r_{\rm H} = k_{\rm meas, H} P_{\rm C_3 H_6} P_{\rm H_2} \tag{2}$$

where  $r_{\rm H}$  is the propene hydrogenation rate and  $k_{\rm meas,H}$  is the second-order hydrogenation rate constant. This equation also shows that the kinetically relevant transition state for hydrogenation contains the same number and type of atoms as a propene and  $H_2$  molecule and a  $H^+$  site, as is also the case for the transition state that mediates monomolecular dehydrogenation (i.e., the same number and type of atoms as in a propane molecule and a  $H^+$  site). The essentially uncovered nature of the protons during both dehydrogenation and hydrogenation reactions and the requisite De Donder relations lead to propane dehydrogenation and propene hydrogenation rates with rate constant ratios that merely reflect the equilibrium constant for the overall dehydrogenation chemical reaction

$$K_{\rm r} = \frac{k_{\rm meas,D}}{k_{\rm meas,H}} \tag{3}$$

( $K_{\rm r}$  is the reaction equilibrium constant; 1.723 kPa at 748 K).<sup>58</sup> The number and/or reactivity of the extrinsic carbonaceous active sites are suppressed at the high H<sub>2</sub> pressures (>60 kPa) and H<sub>2</sub>/C<sub>3</sub>H<sub>6</sub> molar ratios (>1000) used to measure propene hydrogenation rates, as evident in  $k_{\text{meas,H}}$  values for H-MFI-17 that remained essentially invariant (within a factor of 1.2) with time-on-stream at all reactant alkene and H2 pressures and site contact times (Figure S31, SI). The  $k_{\text{meas,H}}$  values (obtained by regression of rate data to the functional form of eq 2) are plotted on the abscissa of Figure 7; these values solely reflect propene hydrogenation at H<sup>+</sup> sites. The dashed line in Figure 7 represents the predicted values of  $k_{\text{meas},D}$  from propane dehydrogenation reactions at  $H^+$  sites, using measured  $k_{\text{meas},H}$ values and  $K_r$  in the manner dictated by eq 3. Values of  $k_{\text{meas,D}}$ measured on the same samples, but at different inlet propane and H<sub>2</sub> pressures (Table 2), are plotted as closed symbols in Figure 7; these values are identical, within the experimental error, to those predicted from measured  $k_{\text{meas,H}}$  values and eq 3,

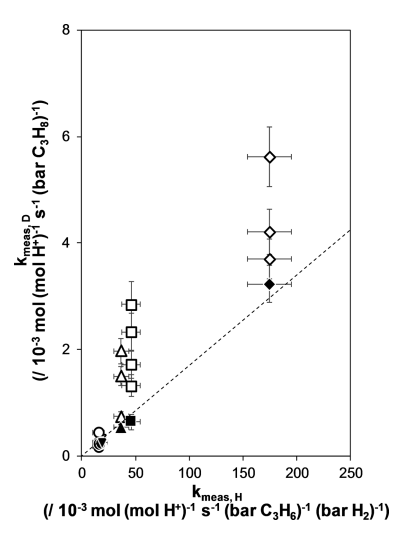


**Figure 7.** Measured second-order rate constants for propene hydrogenation and first-order rate constants for propane dehydrogenation (748 K, per H<sup>+</sup>) on H-MFI-17 (solid diamond), H-MFI-43 (solid square), H-MFI-140 (solid circle), H-MOR-10 (solid up triangle), and H-CHA-16 (solid down triangle) at initial time-onstream with H<sub>2</sub> co-feeds (closed symbols) and at steady-state in the absence of co-fed products (open symbols). The dashed line represents the  $k_{\rm meas,D}$  values predicted from measured  $k_{\rm meas,H}$  values and  $K_{\rm r}$  (0.017 bar)<sup>58</sup> using eq 3.

confirming that propane dehydrogenation rates measured at initial time-on-stream on H-zeolites pretreated in H2 and with H<sub>2</sub> co-feeds solely reflect protolytic reactions. In contrast, propane dehydrogenation rates measured on the same samples at steady state but without co-fed H<sub>2</sub> (Figure S23, SI), after normalization by propane pressure to estimate the values of  $k_{\text{meas,D}}$ , are plotted as open symbols in Figure 7; these values are higher than those predicted from protolytic dehydrogenation reactions at H<sup>+</sup> sites because they also contain additional contributions from dehydrogenation reactions at the extrinsic active sites that do not contribute to hydrogenation rates at the H<sub>2</sub> pressures used for their measurements. Thus, the lower activation energies for propane dehydrogenation estimated from steady-state rate data (Figure 6) are corrupted by additional contributions from lower barrier alkane H-transfer pathways at the carbonaceous active sites.

3.6. Extrinsic Dehydrogenation Sites: Their Role in Discrepancies in Reported Turnover Rates and Activation Barriers and a "Prescription" for Isolating Proton-Catalyzed Dehydrogenation Rates. The initial decrease in dehydrogenation rates during reactions on H-form zeolites treated in O2 (Figure 4a; Figure S21, SI) has also been reported for n-butane dehydrogenation (773-803 K) on H-MFI and H-FAU. 22,28,29 In these studies, dehydrogenation rates reached constant values at shorter times when H-FAU was treated with NH<sub>4</sub>OH to dissolve non-framework Al species, but cracking rates were unaffected by such treatments, leading to the proposal that such extraframework Al species selectively catalyze dehydrogenation before being covered by hydrogen. 22,29 Yet, butane dehydrogenation rates decreased to similar extents (about 5-fold) from initial to steady-state values on both samples, suggesting that the NH<sub>4</sub>OH treatments of H-FAU did not change the number of non-protolytic active sites. The transient decay of dehydrogenation rates to their constant values became longer with decreasing bed residence time,<sup>2</sup> however, consistent with the transient changes in dehydrogenation rates with residence time reported here (Figure S22, SI). Such residence time effects may account for the different transient dehydrogenation rates observed on H-FAU zeolites before and after NH<sub>4</sub>OH treatments. These authors proposed a non-protonic Al site that is intrinsic to the parent aluminosilicate material and its strong titration by H<sub>2</sub> that would be unexpected at the high temperatures (>773 K) and low H<sub>2</sub> pressures (<1 kPa) typical of protolytic activation, as the source of transient decay in alkane dehydrogenation rates at initial time-on-stream before reaching steady-state rates through protolytic reactions.

The role of extraframework Al as an additional dehydrogenation function and its full titration by H<sub>2</sub>, <sup>22</sup> however, are inconsistent with propene formation rates from propane/H<sub>2</sub> mixtures that depend on time-on-stream when 20 kPa H2 is present in the inlet stream (Figures S4-S8, SI); these co-fed H<sub>2</sub> pressures are much higher than product H<sub>2</sub> pressures (<1 kPa) formed from protolytic propane reactions. The previous proposal that non-protolytic active sites are fully inhibited during steady-state dehydrogenation rate measurements seems consistent with their reported first-order dependence on alkane pressure and the absence of product inhibition, 22 but contradicts our findings of the strong inhibition by products of steady-state rates (Figure S23, SI), as well as the excess CH<sub>4</sub> evolved after propane is removed from mixed C<sub>3</sub>H<sub>8</sub>/H<sub>2</sub> reactant streams (Figure S29, SI), which provide compelling evidence for the presence and involvement of organic residues as active sites. The non-equimolar amounts of  $H_2$  and n-butane dehydrogenation products (butenes, butadienes) measured in reactor effluents during the initial time-on-stream reported previously<sup>22</sup> would also be consistent with the formation of carbonaceous deposits during the transient approach to steady state. Such deposits can undergo changes in composition (to change their H/C ratios) in response to the prevalent fluidphase chemical potentials, which may also account for previous findings that H<sub>2</sub> forms for a period of time after n-butane was removed from the inlet stream on H-MFI.<sup>22</sup>

Thus, we interpret the initial transient decrease in dehydrogenation rates after O2 pretreatments and in the absence of co-fed H<sub>2</sub> (Figures 2a and 4a; Figure S21, SI) to arise from the formation of organic residues<sup>59</sup> that evolve in composition as steady-state carbon and hydrogen chemical potentials are attained, to forms that become less effective at catalyzing alkane dehydrogenation. The more gradual increases in dehydrogenation rates at initial time-on-stream with H<sub>2</sub> pretreatments and co-feeds (Figures S4-S8, SI) appear to reflect the slower buildup of unsaturated carbonaceous deposits because the high hydrogen chemical potentials result in hydrogenation of unsaturated organic residues. 44,60 This interpretation is consistent with our findings that the removal of propane from propane/H<sub>2</sub> mixtures results in the removal of unsaturated organic residues to restore H-form zeolites to their states before propane exposure (Figure 4c). Thus, we conclude that H<sub>2</sub> co-feeds mitigate the formation and reactivity of carbonaceous deposits at initial time-on-stream, allowing for measurement of protolytic reaction events.

The effects of bed residence time on *n*-butane dehydrogenation rates for H-MFI zeolites have been previously attributed to competitive binding of alkene products at protons. <sup>26,28</sup> Inhibition of dehydrogenation rates was also observed when *n*-butane reactant streams contained added butenes, which equilibrate over H<sup>+</sup> sites to a mixture of isomers. <sup>28</sup> This proposal led these authors to conclude that the intrinsic

reactivity of protons in these samples could be captured by merely extrapolating dehydrogenation rates to zero residence time to minimize the prevalent concentrations of alkene products.<sup>28</sup> Our data show that, in fact, such an extrapolation to zero residence time leads to the strongest contributions from extrinsic dehydrogenation sites because their reactivity is inhibited significantly by the presence of H2 and alkene products, which exist at their lowest concentrations precisely at such short bed residence times. The proposal of competitive binding of alkene products at protons is also inconsistent with n-butane cracking rates that remained invariant with bed residence time and with co-fed butene pressures in the same report.<sup>28</sup> The subsequent study by Li and co-workers<sup>26</sup> also contradicts the proposal of competitive binding of alkenes at protons, <sup>28</sup> through the direct *in situ* spectroscopic observations that neither the intensity nor the frequency of the acidic OH infrared bands is affected by the same changes to longer bed residence times that led to significantly lower dehydrogenation rates (618-710 K). These authors accurately concluded that a second active site, whose reactivity was inhibited by products, led to additional dehydrogenation events; they did not, however, provide any further insights into the nature or properties of such sites.

Our studies confirm the presence of an extrinsic dehydrogenation function, unrelated to protons, and consisting of organic residues that depend, in number and reactivity, on the carbon and hydrogen chemical potentials in the contacting fluid phase at each point along the catalyst bed. These findings and interpretations "prescribe" the protocols that are required to isolate the contributions from proton-catalyzed dehydrogenation pathways and the turnover rates and kinetic parameters for such protolytic dehydrogenation routes. H-forms of zeolites must be treated in H<sub>2</sub> (803 K, 101 kPa) to remove any adventitious residues formed upon contact with ambient air before use. Rates must be measured in the presence of sufficient H<sub>2</sub> (>20 kPa) in the inlet reactant stream, so as to remove (and/or suppress the formation or reactivity of) any reaction-derived dehydrogenation sites. In situations where H<sub>2</sub> is not co-fed, shorter catalyst beds, lower fluid linear velocities, and higher reactant partial pressures will lead to lower Péclet numbers and to higher extents of back-mixing in catalytic packed beds. Such hydrodynamics minimizes axial gradients in H<sub>2</sub> pressure and, in turn, mitigate the formation and reactivity of the secondary active site, resulting in measured alkane dehydrogenation rates that predominantly reflect protolytic dehydrogenation events, as long as Péclet numbers are not so low that they restrict mass transfer in fluid films external to catalyst particles. Measurements of the reverse propene hydrogenation reaction under conditions that suppress the formation of carbonaceous active sites ( $H_2 > 60 \text{ kPa}$ ,  $H_2/C_3H_6$ > 1000), together with predictions from the De Donder relations of non-equilibrium thermodynamics, should be used to confirm that measured propane dehydrogenation rates indeed reflect only contributions from protolytic reactions.

The broad range of dehydrogenation barriers reported here for propane reactant streams without added H<sub>2</sub> (67–214 kJ mol<sup>-1</sup>; Table 3) resemble those reported in previous studies (65–202 kJ mol<sup>-1</sup>),  $^{9,22-26}$  indicative of the ubiquitous but unrecognized contributions of reaction-derived extrinsic active sites and how time-on-stream, product concentrations, and flow hydrodynamics determine the contributions of such extrinsic sites to measured rates. Only the highest measured propane dehydrogenation barriers (~200 kJ mol<sup>-1</sup>; Table 2)

reflect the true dynamics and energetics of proton-catalyzed monomolecular dehydrogenation routes, a conclusion supported by the consistency of such dehydrogenation rates with those of propene hydrogenation rates through their interconversion thermodynamics (Figure 7); such values of dehydrogenation barriers are higher than for proton-catalyzed monomolecular cracking (by 25–40 kJ mol<sup>-1</sup>) as expected from the different proton affinities of C–H and C–C bonds in propane and their relation to measured activation energies using Born–Haber thermochemical cycles.<sup>9</sup>

Propane dehydrogenation barriers reported here and in earlier studies indicate that barriers are much lower (by up to 100-150 kJ mol<sup>-1</sup>) on the organic residues that account for the extrinsic function than on protons. Measured barriers estimated from steady-state propane dehydrogenation rates in the absence of co-fed H<sub>2</sub> decreased systematically from 202 to 67 kJ mol<sup>-1</sup> with decreasing H<sup>+</sup> density (increasing Si/Al ratio) among H-MFI zeolites and thus with increasing fractions of proton-free voids in these samples. These observations also rationalize the measurement of propane dehydrogenation barriers on the same H-zeolite samples here (H-MFI-17 and H-MOR-10; Table 3) and previously by Gounder and Iglesia<sup>9</sup> at steady state but without co-fed products that are consistent with protolytic dehydrogenation pathways (~200 kJ mol<sup>-1</sup>), because more Al-dense frameworks have fewer proton-free voids available to host unsaturated organic residues that would subsequently contribute to measured dehydrogenation rates. Taken together, these findings indicate that contributions to measured dehydrogenation rates from carbonaceous deposits become more pronounced at lower temperatures and at more dilute Brønsted acid site densities.

The contributions to measured rates from proton-catalyzed routes increase with increasing temperature relative to those from the events mediated by extrinsic sites because of the higher activation barriers for carbonium-ion-mediated routes. As a result, temperature effects on rates can exhibit non-Arrhenius behavior (Figure 6b) as also reported previously for propane dehydrogenation on H-CHA<sup>30</sup> and specifically result in systematically decreasing slopes (and thus measured barriers) at lower temperatures as lower barrier dehydrogenation pathways catalyzed by extrinsic sites become more prevalent. This behavior has been previously attributed to new types of intrinsic active functions formed via Brønsted acid site dehydroxylation during high-temperature (1073 K) treatments in inert environments; such dehydroxylation was proposed to proceed through heterolytic dehydration and homolytic dehydrogenation routes to form H2O and H2, respectively, leaving behind trigonally coordinated Al sites or radical centers at lattice oxygens. 61 MFI zeolites subject to such hightemperature pretreatments and subsequent exposure to naphthalene showed that UV-visible spectral features for radical centers that were taken as evidence to support the proposal for radical sites formed at lattice O atoms upon Brønsted acid site dehydroxylation. 62 These high-temperature inert treatments resulted in measurements of low propane dehydrogenation barriers on H-CHA zeolites (84-174 kJ mol<sup>-1</sup>)<sup>30</sup> but were not used here to reproduce these same low barriers, which are instead attributed to contributions from reaction-derived carbonaceous active sites. These high-temperature inert treatments would also cause any carbonaceous debris present to evolve H2 and become even more unsaturated, potentially leaving behind radical centers on

carbonaceous scaffolds that would participate in alkane dehydrogenation, as proposed here.

Proton-catalyzed alkane dehydrogenation reactions on H-form zeolites were originally reported by Haag and Dessau in 1984; <sup>63</sup> since then, their kinetic details (reaction orders, product inhibition, turnover rates, activation energies, activation entropies) have proven challenging to replicate, with each disparate result fueling a different speculation, whether about the nature of the active function (e.g., non-framework Al) or of the kinetically relevant steps for protolytic pathways. Our body of work provides compelling evidence for extrinsic (reaction-derived) unsaturated carbonaceous deposits as the origin of non-protolytic alkane dehydrogenation catalyzed in parallel to protolytic pathways on acidic zeolites, without requiring the need to disavow the expected kinetic behavior of proton sites.

### 4. CONCLUSIONS

Propane dehydrogenation rates measured on H-form zeolites with co-fed H2 and extrapolated to the time of initial contact with reactants solely reflect protolytic dehydrogenation events, as evidenced by relative barriers for cracking and dehydrogenation that differ by the gas-phase proton affinities of the reactant C-C and C-H bonds and by the strict first-order dependence of rates on alkane pressure without any inhibition effects by H<sub>2</sub> or propene products. Zeolites acquire an extrinsic active site that forms during exposure to propane reactants and their protolytic reaction products. Such extrinsic sites catalyze propane dehydrogenation with much lower barriers than protons and are inhibited by H<sub>2</sub> and propene products, but they do not detectably contribute to cracking products, allowing turnover rates of cracking reactions to serve as a reporter of the state of proton sites during catalysis so long as bimolecular cracking routes do not prevail. The conditions that form extrinsic active sites are characterized by the essential absence of H2, allowing samples to acquire a memory of their sojourn at those conditions. The formation and reactivity of extrinsic sites can be mitigated by high H<sub>2</sub> pressures and H<sub>2</sub>/ alkene ratios, conditions typically used to measure the rates of its reverse reaction (propene hydrogenation), either by the deliberate addition of H<sub>2</sub> to propane reactants or by increasing the axial dispersion using beds with a small Péclet number. Such protocols allow the uncorrupted measurements of the rates and kinetic behavior of proton-catalyzed monomolecular alkane dehydrogenation routes.

These extrinsic active sites do not influence propane cracking rates, which at all conditions occur solely at acidic protons. Such extrinsic active sites consist of unsaturated organic residues with an intermediate affinity for H-atoms that allows them to abstract H-atoms from alkanes and then evolve them as H2; in doing so, they catalyze turnovers but adjust their degree of unsaturation and their affinity for H-atoms in response to the prevalent fluid-phase carbon and hydrogen chemical potentials, via elementary steps that resemble hydrogen transfer events. Such H-transfer processes between bound species and gaseous alkanes and alkenes are ubiquitous in zeolite acid catalysis. The findings reported herein provide specific guidance for depositing, removing, or inhibiting the reactivity of these extrinsic organocatalytic residues that mediate hydrogen transfer reactions via routes that occur in parallel with protolytic routes catalyzed by zeolitic protons.

Alkane dehydrogenation at extrinsic carbonaceous active sites provides a unifying explanation for previous observations

of non-protolytic dehydrogenation events on acidic zeolites, including reports of product inhibition and measurements of activation energies that vary over a wide range and appear to be unrelated to the intrinsic properties of acidic zeolites. Contributions from these reaction-derived sites become more significant at lower temperatures and on zeolites with low H+ site densities, as well as in reactors with strong bed-scale concentration gradients of reaction products that would otherwise selectively inhibit the reactivity of the extrinsic sites. These data and their interpretation illustrate how labscale experimentation under non-differential conditions caused by strong product inhibition leads to hydrodynamic corruptions of kinetic data as a result of the extent of backmixing. Such artifacts cannot be detected or corrected from literature data because of the dearth of details about reactor configurations, extent of mixing, and sample history reported when measuring, reporting, or interpreting data of purported kinetic origin. This prevents the independent reproduction and the retroactive interpretation of data, thus serving to propagate conflicting reports and hypotheses.

## ASSOCIATED CONTENT

## **Supporting Information**

The Supporting Information is available free of charge at https://pubs.acs.org/doi/10.1021/acs.jpcc.0c01808.

XRD patterns,  $N_2$  and Ar adsorption isotherms, transient and steady-state propane cracking and dehydrogenation rates with  $H_2$  and alkene/ $H_2$  co-feeds on H-form zeolites after oxidative and  $H_2$  treatments, evaluation of equilibrium limitations on measured reaction rates, Born—Haber thermochemical cycles for protolytic alkane reactions on zeolites, evaluation of bed-scale  $H_2$  gradients during propane reactions on H-form zeolites, eliminating the role of unsaturated impurities in reactant mixtures on alkane activation rates, transient product formation rates on H-form zeolites after step changes in co-fed  $H_2$ , and steady-state propene hydrogenation rates on H-form zeolites (PDF)

# AUTHOR INFORMATION

## **Corresponding Author**

Rajamani Gounder — Charles D. Davidson School of Chemical Engineering, Purdue University, West Lafayette, Indiana 47907, United States; oorcid.org/0000-0003-1347-534X; Email: rgounder@purdue.edu

#### **Authors**

Philip M. Kester – Charles D. Davidson School of Chemical Engineering, Purdue University, West Lafayette, Indiana 47907, United States

Enrique Iglesia — Department of Chemical and Biomolecular Engineering, University of California at Berkeley, Berkeley, California 94720, United States; orcid.org/0000-0003-4109-1001

Complete contact information is available at: https://pubs.acs.org/10.1021/acs.jpcc.0c01808

#### Notes

The authors declare no competing financial interest.

## ACKNOWLEDGMENTS

The authors acknowledge financial support from the National Science Foundation under Cooperative Agreement no. EEC-1647722 and an Engineering Research Center for the Innovative and Strategic Transformation of Alkane Resources (CISTAR) and support for Prof. Enrique Iglesia from the Neil Armstrong Distinguished Visiting Fellowship (Purdue University). The authors thank Jiahan Xie (UC-Berkeley) for his technical discussions and data collection that assisted in testing the hypotheses and in refining the conclusions described in this manuscript, and Junnan Shangguan (UC-Berkeley) for a critical reading of this manuscript. The authors also thank Neil Razdan (University of Minnesota) and Prof. Aditya Bhan (University of Minnesota) for their helpful technical discussions during the preparation of this manuscript.

## REFERENCES

- (1) Corma, A. Inorganic Solid Acids and Their Use in Acid-Catalyzed Hydrocarbon Reactions. *Chem. Rev.* **1995**, 95, 559–614.
- (2) Tabak, S. A. Oligomerization of Olefins. US4254295A, March 3, 1981.
- (3) Garwood, W. E. Conversion of C2-C10 to Higher Olefins over Synthetic Zeolite ZSM-5. In *Intrazeolite Chemistry*; ACS Symposium Series; American Chemical Society, 1983; Vol. 218, pp 383–396.
- (4) Bellussi, G.; Pazzuconi, G.; Perego, C.; Girotti, G.; Terzoni, G. Liquid-Phase Alkylation of Benzene with Light Olefins Catalyzed by  $\beta$ -Zeolites. *J. Catal.* **1995**, *157*, 227–234.
- (5) Guisnet, M.; Gnep, N. S.; Alario, F. Aromatization of Short Chain Alkanes on Zeolite Catalysts. *Appl. Catal., A* **1992**, 89, 1–30.
- (6) Louis, B.; Pereira, M. M.; Santos, F. M.; Esteves, P. M.; Sommer, J. Alkane Activation over Acidic Zeolites: The First Step. *Chem. Eur. J.* **2010**, *16*, 573–576.
- (7) Greensfelder, B. S.; Voge, H. H.; Good, G. M. Catalytic and Thermal Cracking of Pure Hydrocarbons: Mechanisms of Reaction. *Ind. Eng. Chem.* **1949**, *41*, 2573–2584.
- (8) Kotrel, S.; Knözinger, H.; Gates, B. C. The Haag–Dessau Mechanism of Protolytic Cracking of Alkanes. *Microporous Mesoporous Mater.* **2000**, 35–36, 11–20.
- (9) Gounder, R.; Iglesia, E. Catalytic Consequences of Spatial Constraints and Acid Site Location for Monomolecular Alkane Activation on Zeolites. *J. Am. Chem. Soc.* **2009**, *131*, 1958–1971.
- (10) Gounder, R.; Iglesia, E. Effects of Partial Confinement on the Specificity of Monomolecular Alkane Reactions for Acid Sites in Side Pockets of Mordenite. *Angew. Chem., Int. Ed.* **2010**, *49*, 808–811.
- (11) Gounder, R.; Iglesia, E. The Roles of Entropy and Enthalpy in Stabilizing Ion-Pairs at Transition States in Zeolite Acid Catalysis. *Acc. Chem. Res.* **2012**, *45*, 229–238.
- (12) Gates, B. C. Supported Metal Clusters: Synthesis, Structure, and Catalysis. *Chem. Rev.* **1995**, *95*, 511–522.
- (13) Uzun, A.; Gates, B. C. Dynamic Structural Changes in a Molecular Zeolite-Supported Iridium Catalyst for Ethene Hydrogenation. *J. Am. Chem. Soc.* **2009**, *131*, 15887–15894.
- (14) Weber, W. A.; Zhao, A.; Gates, B. C. NaY Zeolite-Supported Rhodium and Iridium Cluster Catalysts: Characterization by X-Ray Absorption Spectroscopy during Propene Hydrogenation Catalysis. *J. Catal.* **1999**, *182*, 13–29.
- (15) Choi, M.; Wu, Z.; Iglesia, E. Mercaptosilane-Assisted Synthesis of Metal Clusters within Zeolites and Catalytic Consequences of Encapsulation. *J. Am. Chem. Soc.* **2010**, *132*, 9129–9137.
- (16) Zhan, B.-Z.; Iglesia, E. RuO<sub>2</sub> Clusters within LTA Zeolite Cages: Consequences of Encapsulation on Catalytic Reactivity and Selectivity. *Angew. Chem., Int. Ed.* **2007**, *46*, 3697–3700.
- (17) Simon, L. J.; van Ommen, J. G.; Jentys, A.; Lercher, J. A. Sulfur Tolerance of Pt/mordenites for Benzene Hydrogenation: Do Brønsted Acid Sites Participate in Hydrogenation? *Catal. Today* **2002**, *73*, 105–112.

- (18) Minachev, K. M.; Udal'tsova, E. A.; Levitskii, I. I. Hydrogenation of Benzene over NaX and Na-Mordenite Zeolites. *Bull. Acad. Sci. USSR, Div. Chem. Sci.* **1982**, *31*, 301–304.
- (19) Kanai, J.; Martens, J. A.; Jacobs, P. A. On the Nature of the Active Sites for Ethylene Hydrogenation in Metal-Free Zeolites. *J. Catal.* **1992**, *133*, 527–543.
- (20) Heylen, C. F.; Jacobs, P. A.; Uytterhoeven, J. B. Active Sites in Zeolites: 5. Hydrogen-Deuterium Equilibration over Synthetic Faujasites. *J. Catal.* **1976**, 43, 99–110.
- (21) Jacobs, P. A.; Uytterhoeven, J. B. Active Sites in Zeolites: Part 7. Isopropanol Dehydrogenation over Alkali Cation-Exchanged X and Y Zeolites. *J. Catal.* **1977**, *50*, 109–114.
- (22) Narbeshuber, T. F.; Brait, A.; Seshan, K.; Lercher, J. A. Dehydrogenation of Light Alkanes over Zeolites. *J. Catal.* **1997**, *172*, 127–136.
- (23) Xu, B.; Sievers, C.; Hong, S. B.; Prins, R.; van Bokhoven, J. A. Catalytic Activity of Brønsted Acid Sites in Zeolites: Intrinsic Activity, Rate-Limiting Step, and Influence of the Local Structure of the Acid Sites. *J. Catal.* **2006**, *244*, 163–168.
- (24) van Bokhoven, J. A.; Xu, B.Towards Predicting Catalytic Performances of Zeolites. In *Studies in Surface Science and Catalysis*; Xu, R.; Gao, Z.; Chen, J.; Yan, W., Eds.; From Zeolites to Porous MOF Materials The 40th Anniversary of International Zeolite Conference; Elsevier, 2007; Vol. *170*, pp 1167–1173.
- (25) Liu, D.; Bhan, A.; Tsapatsis, M.; Al Hashimi, S. Catalytic Behavior of Brønsted Acid Sites in MWW and MFI Zeolites with Dual Meso- and Microporosity. *ACS Catal.* **2011**, *1*, 7–17.
- (26) Li, H.; Kadam, S. A.; Vimont, A.; Wormsbecher, R. F.; Travert, A. Monomolecular Cracking Rates of Light Alkanes over Zeolites Determined by IR Operando Spectroscopy. *ACS Catal.* **2016**, *6*, 4536–4548.
- (27) Nieminen, V.; Sierka, M.; Murzin, D. Y.; Sauer, J. Stabilities of C3–C5 Alkoxide Species inside H-FER Zeolite: A Hybrid QM/MM Study. *J. Catal.* **2005**, 231, 393–404.
- (28) Janda, A.; Bell, A. T. Effects of Si/Al Ratio on the Distribution of Framework Al and on the Rates of Alkane Monomolecular Cracking and Dehydrogenation in H-MFI. *J. Am. Chem. Soc.* **2013**, 135, 19193–19207.
- (29) Narbeshuber, T. F.; Brait, A.; Seshan, K.; Lercher, J. A. The Influence of Extraframework Aluminum on H-FAU Catalyzed Cracking of Light Alkanes. *Appl. Catal., A* 1996, 146, 119–129.
- (30) Yun, J. H.; Lobo, R. F. Effects of Temperature Pretreatment on Propane Cracking over H-SSZ-13 Zeolites. *Catal. Sci. Technol.* **2015**, *5*, 264–273.
- (31) Di Iorio, J. R.; Gounder, R. Controlling the Isolation and Pairing of Aluminum in Chabazite Zeolites Using Mixtures of Organic and Inorganic Structure-Directing Agents. *Chem. Mater.* **2016**, *28*, 2236–2247.
- (32) Di Iorio, J. R.; Bates, S. A.; Verma, A. A.; Delgass, W. N.; Ribeiro, F. H.; Miller, J. T.; Gounder, R. The Dynamic Nature of Brønsted Acid Sites in Cu–Zeolites During NOx Selective Catalytic Reduction: Quantification by Gas-Phase Ammonia Titration. *Top. Catal.* 2015, 58, 424–434.
- (33) Baerlocher, C.; McCusker, L. B. Database of Zeolite Structures 2008.
- (34) Jones, A. J.; Carr, R. T.; Zones, S. I.; Iglesia, E. Acid Strength and Solvation in Catalysis by MFI Zeolites and Effects of the Identity, Concentration and Location of Framework Heteroatoms. *J. Catal.* **2014**, *312*, 58–68.
- (35) Haag, W. O.; Lago, R. M.; Weisz, P. B. The Active Site of Acidic Aluminosilicate Catalysts. *Nature* **1984**, *309*, 589–591.
- (36) Collins, S. J.; O'Malley, P. J. Density Functional Studies of the Carbonium Ion Species  $CH_5^+$ ,  $C_2H_7^+$  and  $C_3H_9^+$ . Chem. Phys. Lett. 1994, 228, 246–251.
- (37) Esteves, P. M.; Mota, C. J. A.; Ramírez-Solís, A.; Hernández-Lamoneda, R. Potential Energy Surface of the  $C_3H_9^+$  Cations. Protonated Propane. *J. Am. Chem. Soc.* **1998**, *120*, 3213–3219.
- (38) Froment, G. F.; Bischoff, K. B. Chemical Reactor Analysis and Design; Wiley, 1979.

- (39) Guisnet, M.; Magnoux, P. Organic Chemistry of Coke Formation. *Appl. Catal.*, A 2001, 212, 83–96.
- (40) Kyotani, T.; Nagai, T.; Inoue, S.; Tomita, A. Formation of New Type of Porous Carbon by Carbonization in Zeolite Nanochannels. *Chem. Mater.* **1997**, *9*, 609–615.
- (41) Kyotani, T.; Ma, Z.; Tomita, A. Template Synthesis of Novel Porous Carbons Using Various Types of Zeolites. *Carbon* **2003**, *41*, 1451–1459.
- (42) Radwan, A. M.; Kyotani, T.; Tomita, A. Characterization of Coke Deposited from Cracking of Benzene over USY Zeolite Catalyst. *Appl. Catal., A* **2000**, *192*, 43–50.
- (43) Meusinger, J.; Corma, A. Activation of Hydrogen on Zeolites: Kinetics and Mechanism of N-Heptane Cracking on H-ZSM-5 Zeolites Under High Hydrogen Pressure. *J. Catal.* **1995**, *152*, 189–197.
- (44) Arora, S. S.; Shi, Z.; Bhan, A. Mechanistic Basis for Effects of High-Pressure H<sub>2</sub> Cofeeds on Methanol-to-Hydrocarbons Catalysis over Zeolites. *ACS Catal.* **2019**, *9*, 6407–6414.
- (45) Eliason, S. A.; Bartholomew, C. H.Temperature-Programmed Reaction Study of Carbon Transformations on Iron Fischer-Tropsch Catalysts during Steady-State Synthesis. In *Studies in Surface Science and Catalysis*; Bartholomew, C. H.; Fuentes, G. A., Eds.; Catalyst Deactivation; Elsevier, 1997; Vol. 111, pp 517–526.
- (46) Xu, J.; Bartholomew, C. H. Temperature-Programmed Hydrogenation (TPH) and in Situ Mössbauer Spectroscopy Studies of Carbonaceous Species on Silica-Supported Iron Fischer—Tropsch Catalysts. J. Phys. Chem. B 2005, 109, 2392–2403.
- (47) Gräber, W.-D.; Hüttinger, K. J. Chemistry of Methane Formation in Hydrogasification of Aromatics. 1. Non-Substituted Aromatics. *Fuel* **1982**, *61*, 499–504.
- (48) Gräber, W.-D.; Hüttinger, K. J. Chemistry of Methane Formation in Hydrogasification of Aromatics. 2. Aromatics with Aliphatic Groups. *Fuel* **1982**, *61*, 505–509.
- (49) Cerqueira, H. S.; Magnoux, P.; Martin, D.; Guisnet, M. Coke Formation and Coke Profiles during the Transformation of Various Reactants at 450 °C over a USHY Zeolite. *Appl. Catal., A* **2001**, *208*, 359–367.
- (50) Nederlof, C.; Kapteijn, F.; Makkee, M. Catalysed Ethylbenzene Dehydrogenation in CO2 or  $N_2$ —Carbon Deposits as the Active Phase. *Appl. Catal., A* **2012**, *417-418*, 163–173.
- (51) Ba, H.; Tuci, G.; Evangelisti, C.; Ceppatelli, M.; Nguyen-Dinh, L.; Dal Santo, V.; Bossola, F.; Nhut, J.-M.; Rossin, A.; Granger, P.; et al. Second Youth of a Metal-Free Dehydrogenation Catalyst: When γ-Al2O3 Meets Coke Under Oxygen- and Steam-Free Conditions. *ACS Catal.* **2019**, *9*, 9474–9484.
- (52) McGregor, J.; Huang, Z.; Parrott, E. P. J.; Zeitler, J. A.; Nguyen, K. L.; Rawson, J. M.; Carley, A.; Hansen, T. W.; Tessonnier, J.-P.; Su, D. S.; et al. Active Coke: Carbonaceous Materials as Catalysts for Alkane Dehydrogenation. *J. Catal.* **2010**, *269*, 329–339.
- (53) Amano, H.; Sato, S.; Takahashi, R.; Sodesawa, T. Dehydrogenation of Cyclohexene over Carbon Deposited on Alumina. *Phys. Chem. Chem. Phys.* **2001**, *3*, 873–879.
- (54) Reyniers, M.-F.; Beirnaert, H.; Marin, G. B. Influence of Coke Formation on the Conversion of Hydrocarbons: I. Alkanes on a USY-Zeolite. *Appl. Catal., A* **2000**, 202, 49–63.
- (55) Eder, F.; Stockenhuber, M.; Lercher, J. A. Brønsted Acid Site and Pore Controlled Siting of Alkane Sorption in Acidic Molecular Sieves. *J. Phys. Chem. B* **1997**, *101*, 5414–5419.
- (56) De Moor, B. A.; Reyniers, M.-F.; Gobin, O. C.; Lercher, J. A.; Marin, G. B. Adsorption of  $C_2$ – $C_8$  N-Alkanes in Zeolites. *J. Phys. Chem. C* **2011**, *115*, 1204–1219.
- (57) Zheng, X.; Blowers, P. Reactivity of Alkanes on Zeolites: A Computational Study of Propane Conversion Reactions. *J. Phys. Chem. A* **2005**, *109*, 10734–10741.
- (58) Gounder, R.; Iglesia, E. Catalytic Hydrogenation of Alkenes on Acidic Zeolites: Mechanistic Connections to Monomolecular Alkane Dehydrogenation Reactions. *J. Catal.* **2011**, *277*, 36–45.

- (59) Nishihara, H.; Imai, K.; Itoi, H.; Nomura, K.; Takai, K.; Kyotani, T. Formation Mechanism of Zeolite-Templated Carbons. *Tanso* **2017**, *2017*, *169*–174.
- (60) DeLuca, M.; Janes, C.; Hibbitts, D. Contrasting Arene, Alkene, Diene, and Formaldehyde Hydrogenation in H-ZSM-5, H-SSZ-13, and H-SAPO-34 Zeolite Frameworks during MTO. *ACS Catal.* **2020**, *10*, 4593–4607.
- (61) Nash, M. J.; Shough, A. M.; Fickel, D. W.; Doren, D. J.; Lobo, R. F. High-Temperature Dehydrogenation of Brønsted Acid Sites in Zeolites. J. Am. Chem. Soc. 2008, 130, 2460–2462.
- (62) Yun, J. H.; Lobo, R. F. Formation and Evolution of Naphthalene Radical Cations in Thermally Treated H-ZSM-5 Zeolites. *Microporous Mesoporous Mater.* **2012**, *155*, 82–89.
- (63) Haag, W. O.; Dessau, R. M. Proceedings of the 8th International Congress on Catalysis, Berlin, 1984; p 305.